POLITECNICO DI MILANO

School of Industrial and Information Engineering

Master of Science in Automation and Control Engineering

Design and development of a path tracking control and a replanning algorithm for an autonomous vehicle in emergency maneuver

Supervisor: Prof. Sergio Matteo Savaresi

Co-supervisor: Prof. Matteo Corno

Eng. Alex Gimondi

Master Thesis dissertation of:
Edoardo Mori Matr. 900023

Academic year 2018-2019

Dedicated to my family

Ringraziamenti

Innanzitutto, ringrazio il professor *Sergio Savaresi* per avermi dato l'opportunità di lavorare su questo progetto a fianco del gruppo di ricerca mOve. Tra questi un ringraziamento speciale va al professor *Matteo Corno* e al dottorando *Alex Gimondi* per l'assistenza che mi hanno offerto e per la loro pazienza durante questi nove mesi.

Ringrazio la *mia famiglia* per avermi sempre spinto a dare il meglio e per il sostegno datomi in questi cinque anni universitari.

Infine, ringrazio i *miei amici di sempre* che hanno reso più leggeri questi anni di studio e ringrazio i *ragazzi dell'aula tesisti* con cui ho passato tanti bei momenti in questi mesi.

Milano, Dicembre 2019

Edoardo Mori

Contents

Abstract **1**

1 Introduction **5**

1.1 Motivations 5

1.2 State of the Art 7

1.3 Main Contribution 9

1.4 Main Results 10

1.5 Structure of the Thesis 11

2 Vehicle and models description **13**

2.1 Vehicle geometrical and physical description 13

2.2 Actuators characterization 15

2.3 Single-track model 17

2.4 Extension of the single-track model 22

2.4.1 Dependence on the longitudinal velocity 25

2.4.2 Dependence on the friction coefficient 25

2.5 Model of the vehicle in simulation 26

2.6 Definition of maneuvers 27

2.6.1 Double Lane Change 28

2.6.2 Obstacle Avoidance 28

3 Control **31**

3.1 Loop-shaping controller 31
3.1.1 Regulator structure and tuning 32
3.1.2 Sensitivity to velocity and scheduling 33
3.1.3 Feed-forward compensation 37
3.2 Curvature Preview Controller 38
3.2.1 Yaw-rate loop 39
3.2.2 Curvature filter 42
3.2.3 Lateral Error loop 45
3.3 Conclusions 48

4 Controllers results 51
4.1 Comparison of the controllers 51
4.1.1 Double Lane Change 52
4.1.2 Obstacle Avoidance 58
4.2 Sensitivity to the friction coefficient 59
4.3 Conclusions 64

5 Trajectory generation 67
5.1 Sinusoidal lane-change maneuver 67
5.1.1 Choice of f_{ref} 72
5.2 Trajectory replanning 73
5.3 Replanning validation 77
5.3.1 Sensitivity to replanning delay 80
5.4 Conclusions 85

6 Conclusions 87
6.1 Future Work 88

Bibliography 94

List of Figures

1.1 Simplified architecture for fully autonomous drive systems. 6

1.2 Comparison between Curvature Preview and Loop-shaping controllers. Double Lane Change at 90 km/h. 10

1.3 Comparison between Curvature Preview and Loop-shaping controllers. Obstacle Avoidance at 50 km/h. 11

1.4 Comparison between a lane change performed with replanning and one without it. Performed at 90 km/h. Friction coefficient is changed from $\mu = 1$ to $\mu = 0.7$. 12

2.1 Tesla Model X. 14

2.2 Vehicle parameters. 15

2.3 Characteristic curves of electric motors. 16

2.4 Bode plot of G_{mot}. 17

2.5 Bode plot of G_{br}. 18

2.6 Steering system by-wire. 18

2.7 Bode plot of G_{SW}. 19

2.8 Single Track Model. In blue external and inertial forces are highlighted. 19

2.9 Comparison between linear and non-linear tire models. 21

2.10 Lateral positioning error e_{cg} w.r.t. the C.O.G. 23

2.11 $G_{e_{cg}}$ at different velocities. 25

2.12 Sensitivity of $G_{\delta_w \to ecg}(s)$ to the friction coefficient μ. 26
2.13 Some examples of views of CarMaker. 27
2.14 DLC maneuver scheme. 28
2.15 OA maneuver scheme. 29

3.1 Loop-shaping Controller scheme. 32
3.2 Bode plot of $L(s)$. 34
3.3 Sensitivity of $L(s)$ to longitudinal velocity. 35
3.4 Bode plot of the open-loop transfer function $L(s)$ with the scheduling in velocity. 36
3.5 Complete controller scheme with the feed-forward action. 37
3.6 Complete controller scheme with the feed-forward action. 38
3.7 Fourier transforms of the reference maneuvers. 40
3.8 k_r sensitivity analysis on the DLC maneuver. 41
3.9 Sensitivity to k_r of $G_{\rho_{ref} \to e_{cg}}(s)$ at 60 km/h. 42
3.10 Approximation of the transfer function $G_{\rho_{ref} \to e_{cg}}(s)$. 43
3.11 Effect of the curvature reference filtering. 44
3.12 Rearranged control scheme for the design of $R_e(s)$. 46
3.13 Sensitivity to V_x of the open-loop function $R_e(s)G_{\delta_e \to e_{cg}}(s)$. 47
3.14 Sensitivity to V_x of $R_e(s)G_{\delta_e \to e_{cg}}(s)$ with gain scheduling. 48

4.1 Comparison between Curvature Preview and Loop-shaping controllers. DLC. 53
4.2 Simulation on DLC at 30 km/h. 55
4.3 Simulation on DLC at 60 km/h. 56
4.4 Simulation on DLC at 90 km/h. 57
4.5 Comparison between Curvature Preview and Loop-shaping controllers. OA. 58
4.6 Simulation on OA at 60 km/h. 60

4.7 Sensitivity of the tracking performances to different friction coefficients. 61
4.8 DLC simulation using a friction coefficient of $\mu = 0.8$. 62
4.9 DLC simulation using a friction coefficient of $\mu = 0.5$. 63

5.1 Example of sinusoidal lane change maneuver at 50 km/h. 69
5.2 Sensitivity of $G_{\rho_{ref} \to e_{cg}}(s)$ to μ. 72
5.3 Map of the parameter $f_{MAX}(\mu)$. 73
5.4 Example of replanning due to a change in the friction coefficient. . 75
5.5 Comparison between lane change without replanning and with replanning. Change of friction coefficient at the beginning of the lane change from $\mu = 1$ to $\mu = 0.7$. 79
5.6 Comparison between lane change without replanning and with replanning. Change of friction coefficient in the middle of the lane change from $\mu = 1$ to $\mu = 0.7$. 81
5.7 Comparison between lane change without replanning and with replanning. Change of friction coefficient at the beginning of the lane change from $\mu = 1$ to $\mu = 0.5$. 82
5.8 Comparison between lane change without replanning and with replanning. Change of friction coefficient in the middle of the lane change from $\mu = 1$ to $\mu = 0.5$. 83
5.9 Sensitivity of the maneuver performance to different delay τ. Change of friction coefficient at the beginning of the lane change from $\mu = 1$ to $\mu = 0.7$. 85

List of Tables

2.1 Tesla Model X known parameters. 14
2.2 DLC geometrical dimensions. 29
2.3 OA geometrical dimensions. 30

3.1 Loop-shaping controller parameters. 33
3.2 Lateral error regulator's parameters. 47

5.1 Basic solutions used to re-plan the trajectory. 77
5.2 Maximum delays for different replanning simulations. 84

Abstract

In recent years, great technological advances in the automotive sector have been achieved and have allowed guaranteeing higher safety standards, such as ABS and ESP. Despite this, road mortality remains still very high. For this reason, research is working intensively to increase the automation level in vehicles and make them safer.

This thesis, in collaboration with an industrial partner, has two objectives: the first is the realization of a lateral dynamics controller for an autonomous electric vehicle; the second is the development of a trajectory replanning algorithm against sudden changes in road conditions, such as the presence of mud or snow on the road.

After introducing the vehicle and actuator dynamics models, two controllers are designed. The first is based on the lateral error and is enriched by the presence of a feed-forward component which allows a faster action. The second, more sophisticated, is composed of three elements: a regulator that acts on the yaw-rate to keep the vehicle stable, a regulator that has the task of rejecting the lateral error and a filter that allows exploiting the future information on the curvature. Finally, a trajectory replanning algorithm is developed: it is designed to produce a sinusoidal reference coherent with the controller bandwidth and to satisfy more stringent constraints due to a change in the friction coefficient.

Keywords: autonomous drive, path tracking, trajectory replanning, vehicle dynamics

Sommario

Negli ultimi anni, sono stati raggiunti grandi progressi tecnologici nel settore automobilistico che hanno permesso di garantire standard di sicurezza più elevati, come l'ABS e l'ESP. Nonostante ciò, la mortalità stradale rimane ancora molto elevata. Per questo motivo, la ricerca è intensamente impegnata allo sviluppo di maggiori livelli di automazione nei veicoli con il fine di renderli più sicuri.

Questa tesi si prefigge due obiettivi: il primo è la realizzazione su un veicolo elettrico autonomo di un controllore della dinamica laterale; il secondo è quello di sviluppare un algoritmo di ripianificazione della traiettoria a fronte di cambi improvvisi delle condizioni stradali, come la presenza di fango o neve sulla strada.

Dopo aver introdotto i modelli della dinamica del veicolo e degli attuatori, vengono realizzati due controllori. Il primo è basato sull'errore laterale ed è arricchito dalla presenza di un componente *feed-forward* che permette un'azione più rapida. Il secondo, più sofisticato, è composto di tre elementi: un regolatore che agisce sullo *yaw-rate* per mantenere il veicolo stabile, un regolatore che ha il compito di reiettare l'errore laterale e un filtro che permette di sfruttare informazioni future sulla curvatura. Infine, viene sviluppato un algoritmo di ripianificazione della traiettoria in grado di generare un riferimento sinusoidale coerente con la banda del controllore e di soddisfare i vincoli più rigorosi dovuti a una modifica del coefficiente di attrito.

Parole chiave: guida autonoma, inseguimento della traiettoria, ripianificazione della traiettoria, dinamica del veicolo

Chapter 1

Introduction

1.1 Motivations

It is estimated that in 2010 it was reached one billion circulating vehicles ([1]) and this number will be doubled in 2035. Cars represent the primary means of transport, however, every year in the world about 35 million people are injured and about 1.35 million die for road accidents, that is estimated as the eighth leading cause of death for people of all the ages and the first for children and young people ([2]).

Many steps to increase road safety were already done in the past and, nowadays, the cars are equipped with various sensors and electronic systems to assist the driver during both normal navigation and emergencies. Citing some of these technologies: the ABS and ESP have incredibly reduced the number of road victims. Those advances in technologies reduced the accidents but still the number of fatalities and injuries is too high, mainly due to human errors. However, with the evolution of more sophisticated global positioning system (GPS) technologies and the increasing presence in cars of sensors, cameras and by-wire actuators, there are new opportunities for more advanced autonomous driving systems, which have become an increasingly popular topic for both academic and

industrial sectors.

A generic autonomous driving system can be represented with a simplified scheme, such as the one in Figure 1.1, that includes different hierarchical levels. The information from the GPS, together with pre-stored maps, can be exploited by a higher motion planner to generate a feasible path and a maneuver to perform. Then, the trajectory planner has to realize an obstacle-free reference accordingly to the vehicle constraints. The trajectory information is passed to a path tracking controller that acts on many actuators (e.g. steering wheel, brakes and motors) to keep the vehicle as close as possible to the given path reference. Finally, the signals from the path tracking module are passed to lower-level control systems, such as ABS and ESP. Sensors and cameras are then used to determine the vehicle state and to sense the environment.

This thesis dissertation, in collaboration with an industrial partner, deals with two aspects in particular: the control of the lateral dynamics of the vehicle, by acting on the steering wheel, and the trajectory replanning. In particular, the analysis is focused on the emergency maneuvers and it is studied the effect of the friction coefficient on the car behavior.

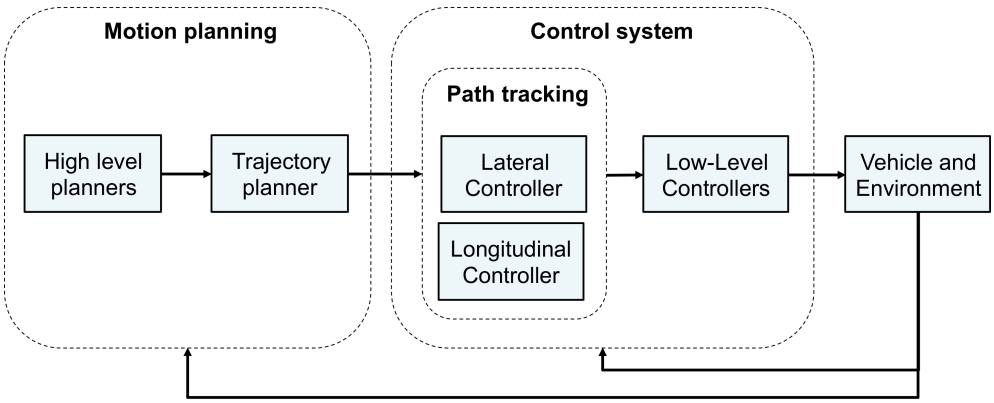

Figure 1.1: Simplified architecture for fully autonomous drive systems.

1.2 State of the Art

Path following and trajectory replanning constitute two important functions of a self-driving car and a huge variety of strategies have been proposed in the literature for both the tasks.

The path following is becoming increasingly relevant for guaranteeing safety on autonomous cars. Several methods have been presented depending on the studied application: urban driving, racing and emergency maneuvers. Urban driving is not particularly demanding from the point of view of the path following controller since the kinematic model is sufficient to describe the vehicle dynamics and the tire sliding is limited. For this purpose some approaches based on the kinematic model were presented in the DARPA Urban Challenge [3] and other methods derived from the robotics were described by [4]. The urban context is, however, out of the scope of this thesis.

More interesting are the emergency maneuvers and racing scenarios. These are more dynamically challenging so the kinematic model does not describe accurately the vehicle: the dynamics produced by the mass and the moment of inertia cannot be neglected anymore and the side slips at the wheels are not negligible. The current research on path tracking is focused to improve the controllers in these situations and different strategies were proposed.

In [5] it was used a linear single-track model extended with a parameter to take account of the tire non-linearity and it was proposed a controller composed of three components: a yaw-damping contribute to avoids yaw oscillations; a feed-forward steering command, based on the linear bicycle model, and a feed-back steering command based on a potential field lane-keeping system, which exploits the future information of the error with respect the given trajectory. In [6] it was reduced the nonlinear model complexity introducing the Center of Percussion (COP) and using a differential flatness technique. In [7] it is modeled a virtual driver using an Optimal Preview Controller; with this technique, the

steering command is chosen as a function of the error that will be committed in the future. In [8] a similar methodology is used and different vehicle settings are identified and the behavior of the virtual driver is determined by weights associated with the future path at several look-ahead distances. A key factor is the exploitation of future information on the maneuver: preview-based controllers are often designed with Model Predictive Control (MPC) strategies since the future point of the trajectory can be easily introduced in the problem formulation. Some first attempts to use MPC to path following of emergency maneuvers are found in [9]. More recent works using MPC on non-linear models of the vehicle can be found in [10], [11], [12] and [13]. In [14], driving data are collected and used to calibrate uncertain models that are exploited in a stochastic MPC (SMPC) scheme. [15] uses an MPC approach and defines a path geometry change (PGC) index to determine the severity of the maneuver and to set the length of the MPC horizon. Despite these approaches perform well in simulations, the real-time application is most of the times not feasible due to the burden of the high computational effort. For this reason, in this thesis, the control strategy explained in [16] is used: it exploits the future information of the given trajectory but does not use optimization techniques.

There are different trajectory generation and replanning methods in the literature. Some approaches use cell decomposition algorithms, such as Rapidly-exploring Random Tree ([17]) that can incorporate kinetic vehicle constraints but have difficulties in taking account of dynamic ones. Other methods exploit potential field algorithms, which are based on the design of repulsive fields to obstacles and attractive fields to safe areas and then the computation of trajectories along the steepest gradient ([18] and [19]). These techniques suffer of a high computational cost and others preferred to use curves belonging to specific classes of functions like polynomials ([20],[21],[22]), splines ([23],[24],[25]) or clothoids ([26]).

These methods are considering the static limits of the maximum acceleration

and the kinetic constraints of the vehicle, which is working in normal driving conditions. However, in emergency maneuvers, the path tracking controller might be unable to track the given trajectory if the dynamic limitations are not considered. Some approaches that solve this problem can be found in the literature and these are mainly based on the unification of the path planning and path tracking modules. MPC is used by [27] and [28] to realize a single module that both stabilizes the vehicle and avoids the obstacles on low-curvature roads. In [29] a mediation between keeping the vehicle stable and avoiding the obstacles is performed.

However, the problem of these approaches is the realization of a complicate unified controller which is difficultly to integrate with other software components of the vehicle. In this thesis is followed the planning strategy found in [16], which maintains the duality of the path tracking and path planning modules but also considers the dynamic constraints of the vehicle. This is done by taking into account the bandwidth of the lateral dynamics controller.

1.3 Main Contribution

The principal contribution of this thesis is a completion of the work of [16] by analyzing the robustness of his tracking controller and by proposing a modification to the emergency replanning strategy to deal with unexpected grip changes.

The controller, which will be called Curvature Preview Controller, acts on the steering actuator and it can be divided into three elements: a regulator that acts on the yaw-rate to stabilize the vehicle, a regulator that has the task of rejecting the error with respect the given trajectory and a component which filters the curvature to exploit the future information of the trajectory. This last component is of key importance to obtain good results, in particular in the emergency maneuvers.

The replanning strategy is realized starting from a trajectory generation algorithm that can build lane-change maneuvers, coherently with the limitations on

the maximum curvature and controller bandwidth. The replanning considers the vehicle state and has the aim to reduce the risk due to the unexpected presence on the road of mud or snow.

1.4 Main Results

The Curvature Preview controller is compared with a controller, designed using classic loop-shaping techniques, at different speeds on two reference maneuvers: the Double Lane Change and the Obstacle Avoidance. While the trajectory replanning algorithm is tested on lane changes using different friction coefficients.

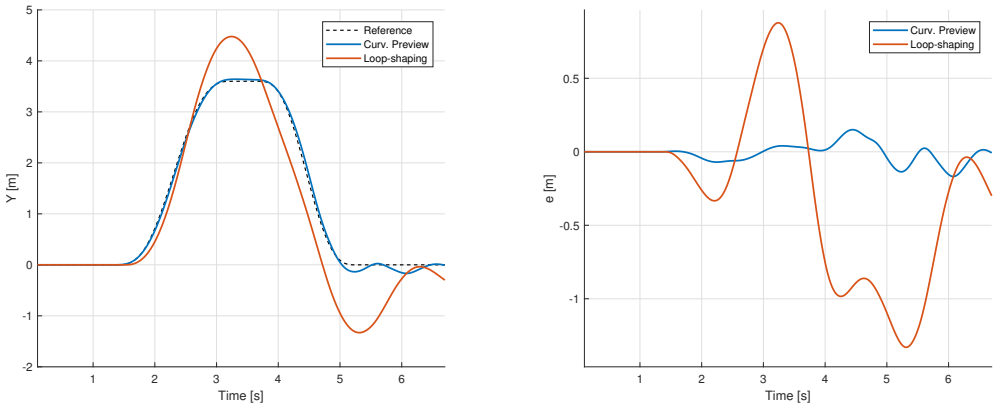

(a) Maneuver comparison.

(b) Lateral error comparison.

Figure 1.2: Comparison between Curvature Preview and Loop-shaping controllers. Double Lane Change at 90 km/h.

The Curvature Preview Controller gives better results with respect to the Loop-Shaping controller and keeps small lateral error also at the highest speeds. The Double Lane Change is correctly performed in nominal conditions up to 90 km/h (Fig. 1.2a), to which corresponds a lateral error of only 0.17 m (Fig. 1.2b); while the Obstacle Avoidance maneuver (Fig. 1.3a) can be performed safely up to 50 km/h, to which corresponds a lateral error of 0.23 m (Fig. 1.3b).

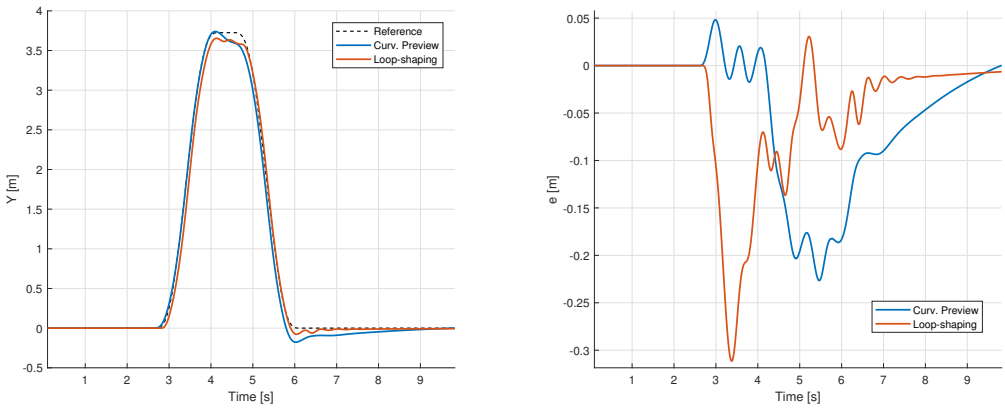

(a) Maneuver comparison.

(b) Lateral error comparison.

Figure 1.3: Comparison between Curvature Preview and Loop-shaping controllers. Obstacle Avoidance at 50 km/h.

The replanning algorithm is proved to give benefits to road safety in case of unexpected grip changes: for example, even if at high speed the vehicle can be kept stable after the friction changed from $\mu = 1$ to $\mu = 0.7$ (Fig. 1.4). Moreover, an analysis of the parameters that affect the success of the replanned maneuver is conducted: in particular the entity of the friction change and the maximum delay to detect the event.

1.5 Structure of the Thesis

This thesis dissertation is structured as follows:

- in **Chapter 2** the experimental setup is presented with all the geometric and physical parameters of the vehicle and the characterization of the models which are going to be used in the other chapters;
- in **Chapter 3**, firstly, the Loop-shaping controller, that is used as a benchmark, is presented and, after, the Curvature Preview Controller is introduced and designed. Both the controllers will be scheduled in velocity;

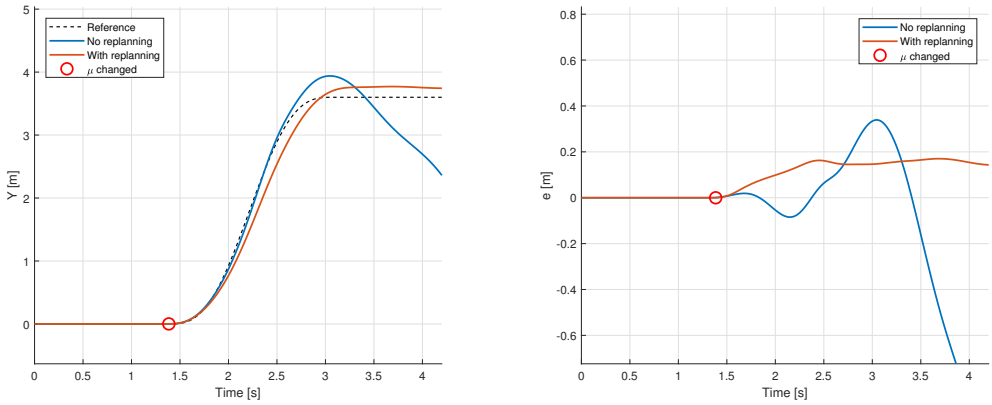

(a) Maneuver comparison.

(b) Lateral error comparison.

Figure 1.4: Comparison between a lane change performed with replanning and one without it. Performed at 90 km/h. Friction coefficient is changed from $\mu = 1$ to $\mu = 0.7$.

- in **Chapter 4** the comparison between the two controllers is discussed using two emergency maneuvers as references and a sensitivity to the variation of the friction coefficient is analyzed;
- in **Chapter 5** an algorithm for the generation of trajectories satisfying constraints on maximum curvature, controller bandwidth and friction is introduced. Moreover, it is extended with a replanning strategy that improves the safety of the vehicle;
- in **Chapter 6** the conclusions are reported and a hint towards future possible research work is given.

Chapter 2

Vehicle and models description

This chapter introduces the vehicle considered for the development of the control systems. The first section describes the geometric and physical parameters of the car. While, in the second section, the main actuators are characterized: the electric motors, the brakes and the steering-by-wire actuator. In the third and the fourth sections, a single-track model is used to describe the lateral dynamics of the vehicle and, then, the single-track extended with the lateral error model will be derived. A sensitivity analysis of this model to the friction coefficient is also conducted. In the fifth section the simulation software CarMaker, which is used to validate the control strategies and the trajectory replanning, is presented. The last section describes the reference maneuvers and gives their geometric definitions.

2.1 Vehicle geometrical and physical description

The vehicle used in the simulations is a modified Tesla Model X (Fig. 2.1) characterized by the geometrical and physical dimensions reported in Table 2.1. The industrial partner, with whom the thesis is in collaboration, provided all the vehicle parameters.

Figure 2.1: Tesla Model X.

Table 2.1: Tesla Model X known parameters.

Mass	m	2602	kg
Wheelbase	L	2.965	m
Vehicle Width	w_v	1.999	m
Front semi-wheelbase	l_f	1.522	m
Rear semi-wheelbase	l_r	1.443	m
C.O.G. height	h_{cg}	0.51	m
Vertical mass moment of inertia	J_z	2700	$\mathrm{kg} \cdot \mathrm{m}^2$
Steering ratio	i_{SW}	14.1	–
Front cornering stiffness	C_f	155000	N/rad
Rear cornering stiffness	C_r	205000	N/rad

In Figure 2.2 the principal dimensions are shown graphically. The parameter i_{SW} represents the ratio between the angle of the steering wheel δ_{SW} and the

steering angle δ_w (which is the average steering angle between left and right wheels):

$$i_{SW} = \frac{\delta_{SW}}{\delta_w} \tag{2.1}$$

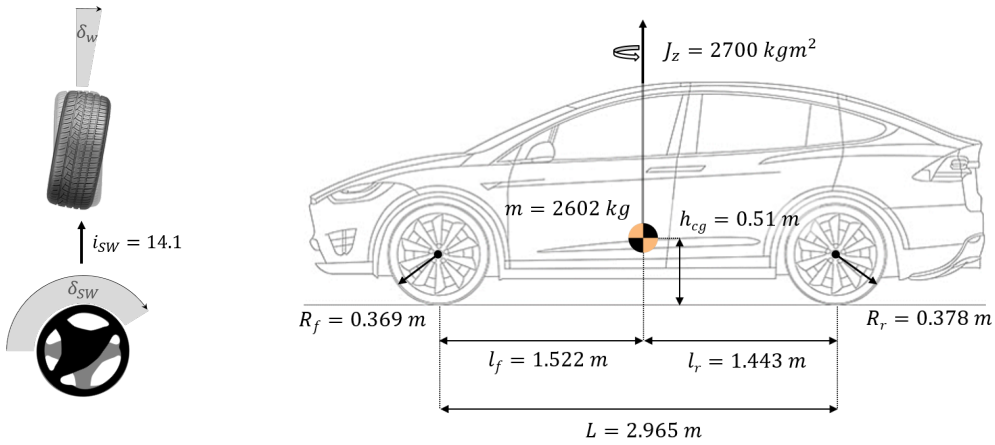

(a) Steering ratio.

(b) Relevant geometrical and physical parameters.

Figure 2.2: Vehicle parameters.

2.2 Actuators characterization

The considered actuators are: the motors and the brakes, which are used in the longitudinal control part, and the steering wheel, which is used for the lateral control and is fundamental for the path tracking task.

The vehicle has four independent electric motors, one per wheel, and it is assumed that the motors can be controlled to exert both positive (traction) and negative (braking) torques. A map of the characteristic curves for both front and rear electric motors is provided. In Figure 2.3 the maximum traction output torque together with the regenerative braking torque are shown at different motor speeds (Fig. 2.3a shows the front motors curves, while Fig. 2.3b the rear ones).

The torque that can be requested to the motors is limited by the characteristic curves but it must also consider the dependence between the requested torque

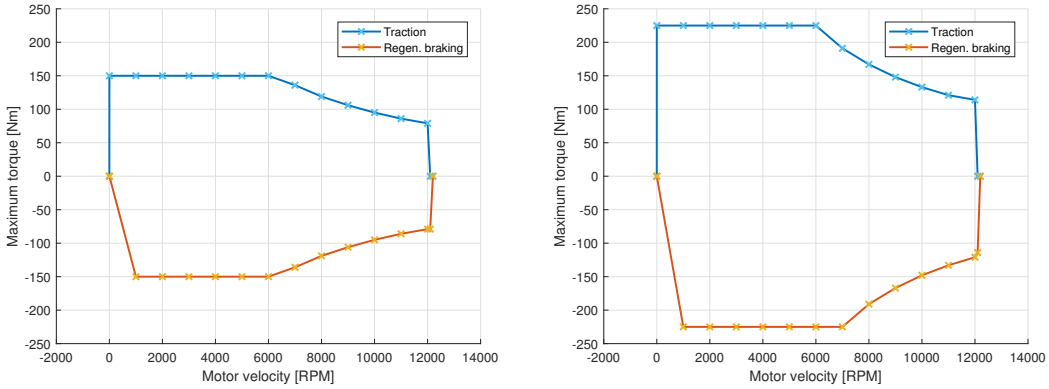

(a) Front motors. (b) Rear motors.

Figure 2.3: Characteristic curves of electric motors.

signal and the response of the motor. To this scope, such model is assumed known and it is defined as a first-order model with an actuation delay of 0.01 s:

$$G_{mot}(s) = \frac{1}{\frac{s}{2\pi 20} + 1} \mathrm{e}^{-0.01s} \tag{2.2}$$

where the pole is situated at 20 Hz. In Figure 2.4 the transfer function magnitude and phase are reported.

Similarly, also the brakes are characterized by a first-order model and by an actuation delay; in this case the pole is in 10 Hz:

$$G_{br}(s) = \frac{1}{\frac{s}{2\pi 10} + 1} \mathrm{e}^{-0.01s} \tag{2.3}$$

This transfer function represents the dependence between the brake position reference and the actual response of the brakes. The bode plot of this transfer function is shown in Fig. 2.5.

The steering actuator mounted on this vehicle is described and identified by [16]. The steer-by-wire system is composed by an electric motor directly connected through a belt transmission to the steering column as shown in Figure 2.6. This actuator has an embedded control system that deals with the tracking of the reference position sent by the vehicle control system. The model which describes

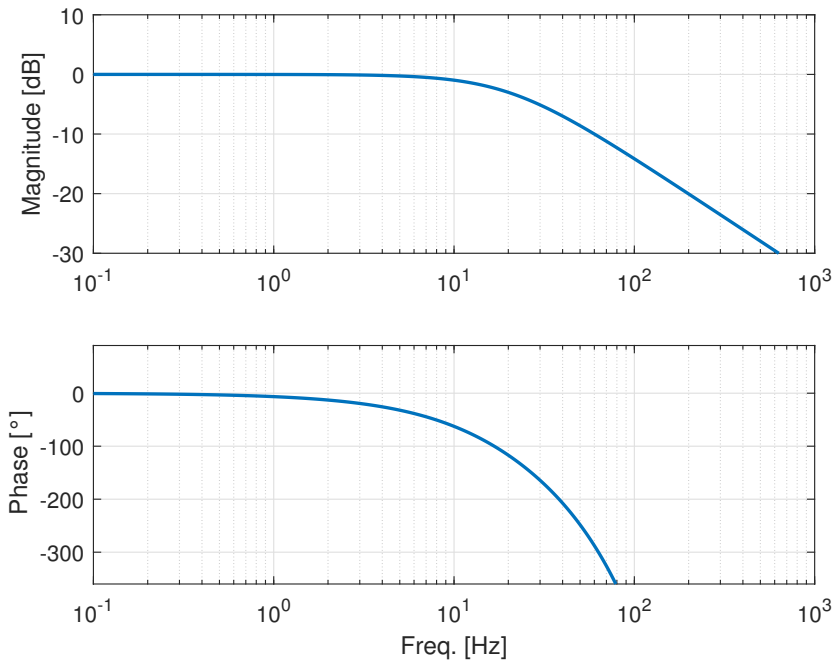

Figure 2.4: Bode plot of G_{mot}.

the relation between the requested angle of the steering wheel and the actuated one is:

$$G_{SW}(s) = \frac{(2\pi 4.1)^2 \mathrm{e}^{-0.08s}}{s^2 + s0.203(2\pi 4.1) + (2\pi 4.1)^2} \tag{2.4}$$

The steering actuator can't be neglected when the path tracking controller will be designed since the time delay (of 0.08 s) and the resonance (Fig. 2.7) have effect inside the desired control bandwidth (about 1 Hz).

2.3 Single-track model

In this section, the lateral dynamics of the vehicle is represented with a linear single-track model (Fig. 2.8), which is very well explained in the literature, such as in [30]. This model allows the approximate, yet physically plausible, description of the lateral dynamics of a vehicle.

The underlying assumptions of the model are the following:

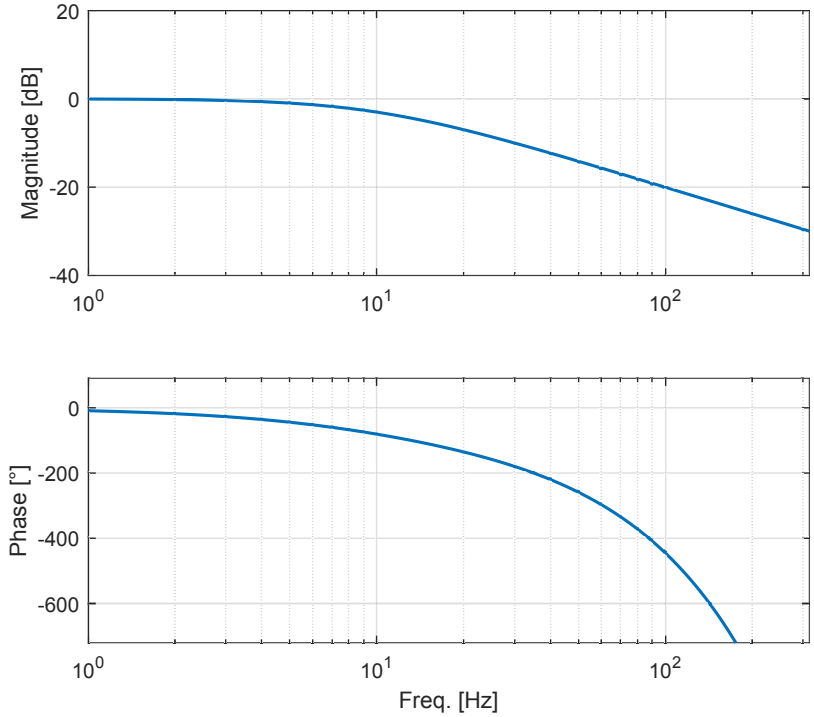

Figure 2.5: Bode plot of G_{br}.

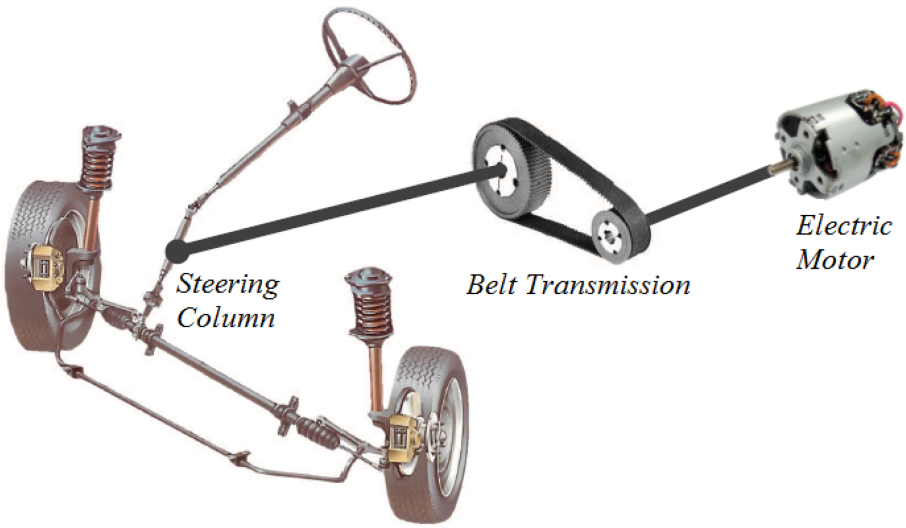

Figure 2.6: Steering system by-wire.

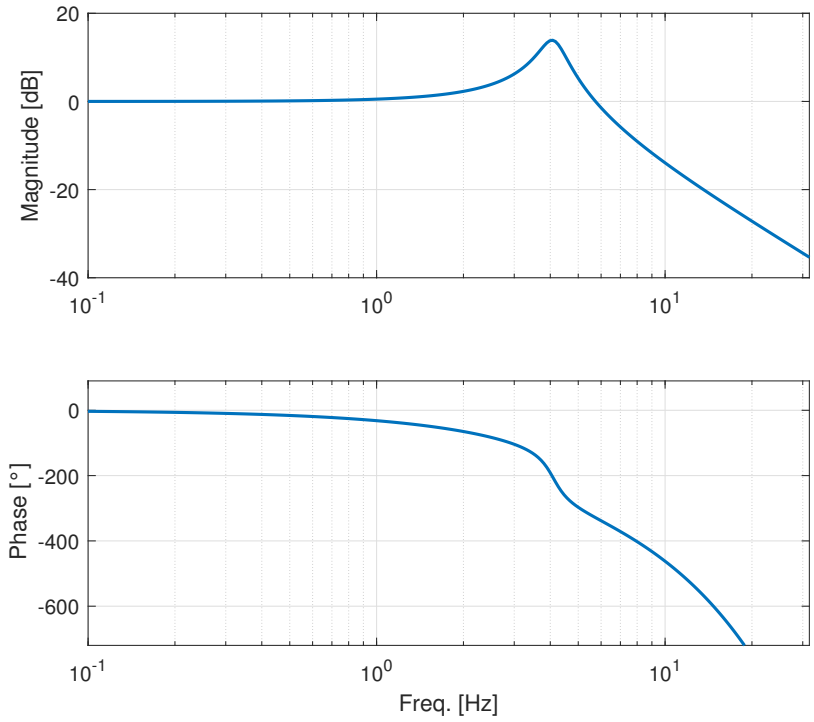

Figure 2.7: Bode plot of G_{SW}.

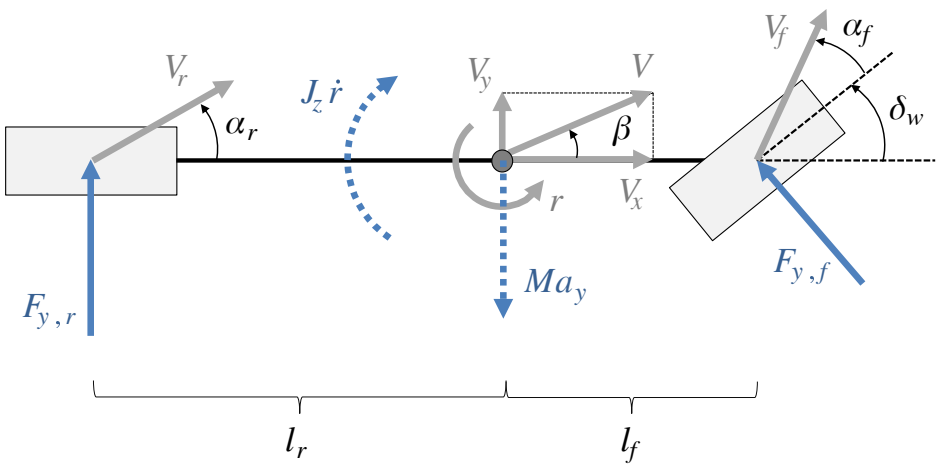

Figure 2.8: Single Track Model. In blue external and inertial forces are highlighted.

1. left and right wheels are lumped into a front and a rear wheel in the centerline of the car, therefore this model is also known as "bicycle model";
2. negligible roll dynamics and weight transfer;
3. horizontal velocity V_x is supposed constant;
4. the mass of all the vehicle is concentrated in the center of gravity (C.O.G.);
5. small slip angles β, α_r and α_f and small steering angle δ_w;
6. traction and braking forces are considered small with respect to the lateral tire forces $F_{y,f}$ and $F_{y,r}$;
7. aerodynamics forces are neglected;
8. linear tire characteristics.

Despite its simplicity this vehicle model allows the investigation of the fundamental driving dynamic relationships within the lateral acceleration region of:

$$a_y <= 0.4g \approx 4\frac{\mathrm{m}}{\mathrm{s}^2} \tag{2.5}$$

on dry roads ([30]).

The equations of motion are derived from the lateral force and moment balance:

$$\begin{aligned} ma_y = m(\dot{V}_y + rV_x) &= F_{y,r} + F_{y,f}\cos\delta_w \\ J_z\dot{r} &= l_f F_{y,f}\cos\delta_w - l_r F_{y,r} \end{aligned} \tag{2.6}$$

where a_y is the lateral acceleration, V_y is the lateral velocity, r is the yaw rate.

The lateral tire forces highly influence the dynamics of the vehicle and the entity of those is dependent on the slip angles of the tires. There are different ways to model those forces, both linear or nonlinear. A non-linear model, for example the Pacejka model (which is explained in [31]) considers the saturation of the tires at high slip angles (this typically happens when the lateral accelerations are

higher than $a_y > 0.4g$). The linear model, instead, well describes the tire behavior at low slip angles and at low lateral accelerations. A comparison between linear and non-linear tire models is reported in Fig. 2.9.

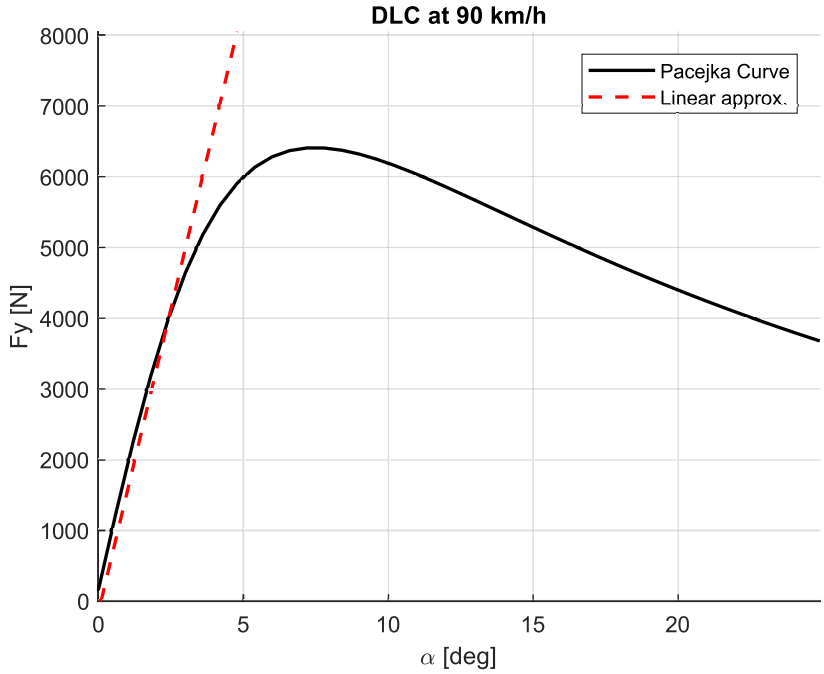

Figure 2.9: Comparison between linear and non-linear tire models.

However, as anticipated in the assumptions, a linear tire model is used during the theoretical analysis. Thus it is possible to express the lateral tire forces as linear functions of the rear and front tire slip angles (respectively α_r and α_f):

$$\begin{aligned} F_{y,r} &= -C_r \alpha_r \\ F_{y,f} &= -C_f \alpha_f \end{aligned} \tag{2.7}$$

where C_r is the cornering stiffness of the rear axle and C_f is the cornering stiffness of the front axle.

The slip angles α_r and α_f can be expressed as:

$$\begin{aligned} \alpha_r &= \arctan\left(\frac{V \sin\beta - l_r r}{V \cos\beta}\right) \\ \alpha_f &= -\delta_w + \arctan\left(\frac{V \sin\beta + l_f r}{V \cos\beta}\right) \end{aligned} \tag{2.8}$$

and exploiting the small slip angle assumption it is possible simplify writing:

$$\begin{aligned} \alpha_r &= +\beta - \frac{l_r r}{V_x} \\ \alpha_f &= -\delta_w + \beta + \frac{l_f r}{V_x} \end{aligned} \tag{2.9}$$

thus equations 2.7 become:

$$\begin{aligned} F_{y,r} &\approx -C_r \left(\frac{V_y - r l_r}{V_x} \right) \\ F_{y,f} &\approx -C_f \left(\frac{V_y - r l_f}{V_x} - \delta_w \right) \end{aligned} \tag{2.10}$$

Using the tire forces equations 2.10 and the equations of motion of the vehicle 2.6, the following system in matrix notation is obtained:

$$\begin{bmatrix} \dot{V}_y \\ \dot{r} \end{bmatrix} = \begin{bmatrix} -\frac{C_f + C_r}{m V_x} & \frac{C_r l_r - C_f l_f}{m V_x} - V_x \\ \frac{C_r l_r - C_f l_f}{J_z V_x} & -\frac{C_r l_f^2 + C_r l_r^2}{J_z V_x} \end{bmatrix} \begin{bmatrix} V_y \\ r \end{bmatrix} + \begin{bmatrix} \frac{C_f}{m} \\ \frac{C_f l_f}{J_z} \end{bmatrix} \delta_w \tag{2.11}$$

The model obtained is a second-order dynamic system with a single input, the steering angle δ_w. Note that in this dissertation the horizontal velocity will be considered as a varying parameter with much slower dynamics compared with the lateral one. Thus the assumption of constant horizontal velocity is still valid.

2.4 Extension of the single-track model

The model found describes the dynamics in terms of lateral velocity V_y and yaw rate r. Now the path tracking problem has to be included in the model. For this reason, the single-track model is now extended with the states e_{cg} and $\Delta\psi$. They represent respectively the lateral positioning error with respect to the C.O.G. (Fig. 2.10) and the difference between the yaw angle of the vehicle and trajectory angle, which can be defined as the heading error.

The formulation that is used to define the extension of the single-track system can be found for example in [32]. The reference path is described by the

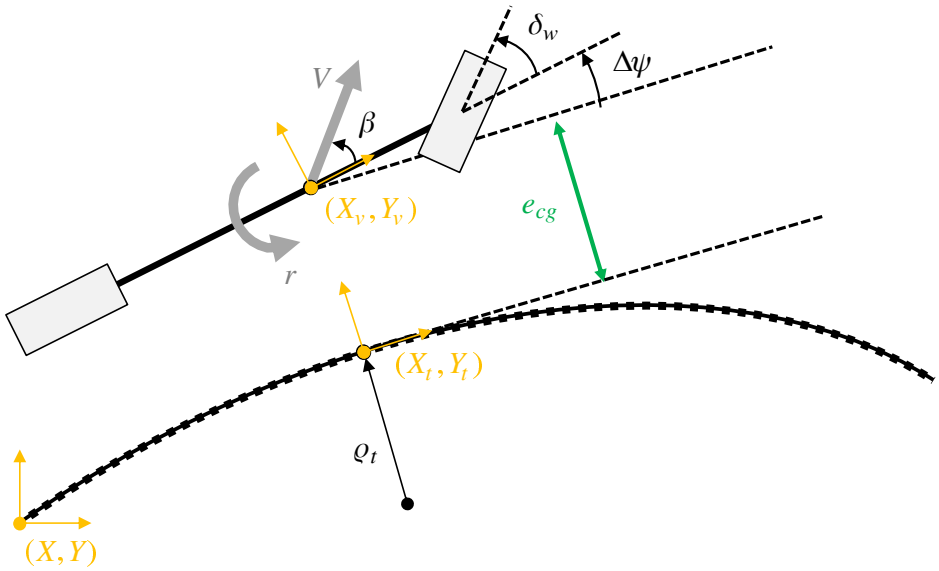

Figure 2.10: Lateral positioning error e_{cg} w.r.t. the C.O.G.

coordinates X_t and Y_t and the curvature ρ_t. The road curvature and the reference longitudinal speed (V_t) determines the rate of change of the desired vehicle orientation:

$$\dot{\psi}_t = \rho_t V_t \approx \rho_t V_x \tag{2.12}$$

where it is assumed that the reference speed V_t is perfectly tracked and thus $V_x \approx V_t$. Thus the dynamics of the heading error is given by:

$$\dot{\Delta\psi} = r - \dot{\psi}_t = r - \rho_t V_t \approx r - \rho_t V_x \tag{2.13}$$

The derivative of the lateral error is given by the following expression:

$$\dot{e}_{cg} = V_y \cos \Delta\psi + V_x \sin \Delta\psi \tag{2.14}$$

Using the small angle assumptions we can simplify 2.14 and 2.13 by writing:

$$\begin{aligned} \dot{e}_{cg} &= V_y + V_x \Delta\psi \\ \dot{\Delta\psi} &= r - \rho_t V_x \end{aligned} \tag{2.15}$$

The state-space representation for path tracking control is derived by adding these two equations to the single track model 2.11 and by considering e_{cg} as

output of the system:

$$\begin{bmatrix} \dot{V}_y \\ \dot{r} \\ \dot{\Delta\psi} \\ \dot{e}_{cg} \end{bmatrix} = \begin{bmatrix} -\frac{C_f+C_r}{mV_x} & \frac{C_r l_r - C_f l_f}{mV_x} - V_x & 0 & 0 \\ \frac{C_r l_r - C_f l_f}{J_z V_x} & -\frac{C_r l_f^2 + C_r l_r^2}{J_z V_x} & 0 & 0 \\ 0 & 1 & 0 & 0 \\ 1 & 0 & V & 0 \end{bmatrix} \begin{bmatrix} V_y \\ r \\ \Delta\psi \\ e_{cg} \end{bmatrix} + \begin{bmatrix} \frac{C_f}{m} & 0 \\ \frac{C_f l_f}{J_z} & 0 \\ 0 & -V_x \\ 0 & 0 \end{bmatrix} \begin{bmatrix} \delta_w \\ \rho_t \end{bmatrix}$$

$$y = \begin{bmatrix} 0 & 0 & 0 & 1 \end{bmatrix} \begin{bmatrix} V_y \\ r \\ \Delta\psi \\ e_{cg} \end{bmatrix} \tag{2.16}$$

The reference curvature ρ_t appears as an exogenous disturbance to the system, the lateral error e_{cg} is the variable that we want to control and output of the system and, finally, the steering angle δ_w is the control variable.

Given the state-space representation, the following transfer functions from the inputs to the output of the system can be obtained:

- between the steering angle δ_w and the lateral error e_{cg}

$$G_{\delta_w \to ecg}(s) = \frac{V_x}{s^2} \frac{\tilde{N}(s)}{\tilde{D}(s)} \tag{2.17}$$

  where:

$$\begin{aligned} \tilde{N}(s) =& C_f J_z V_x s^2 + (C_f C_r l_r^2 + C_f C_r l_f l_r)s + C_f C_r (l_r + l_f) V_x \\ \tilde{D}(s) =& J_z m V_x^2 s^2 + [(C_f + C_r) J_z + (C_f l_f^2 + C_r l_r^2) m] V_x s + \\ & + C_f C_r (l_f + l_r)^2 + (C_r l_r - C_f l_f) m V_x^2 \end{aligned} \tag{2.18}$$

- between the curvature reference ρ_t and the lateral error e_{cg}

$$G_{\rho_t \to ecg}(s) = -\frac{V_x}{s^2} \tag{2.19}$$

The control strategies will be designed based on these two transfer functions.

2.4.1 Dependence on the longitudinal velocity

The emergency maneuvers used in this thesis will be tested at a wide range of velocities therefore the dependence of the vehicle model $G_{\delta_w \to ecg}(s)$ to the longitudinal speed V_x is crucial. Figure 2.11 represents how $G_{e_{cg}}(s)$ varies changing V_x and it can be concluded that the main difference is in the bandwidth of the model. This variability will be taken in account during the design of the controllers and an appropriate scheduling strategy will be explained and applied.

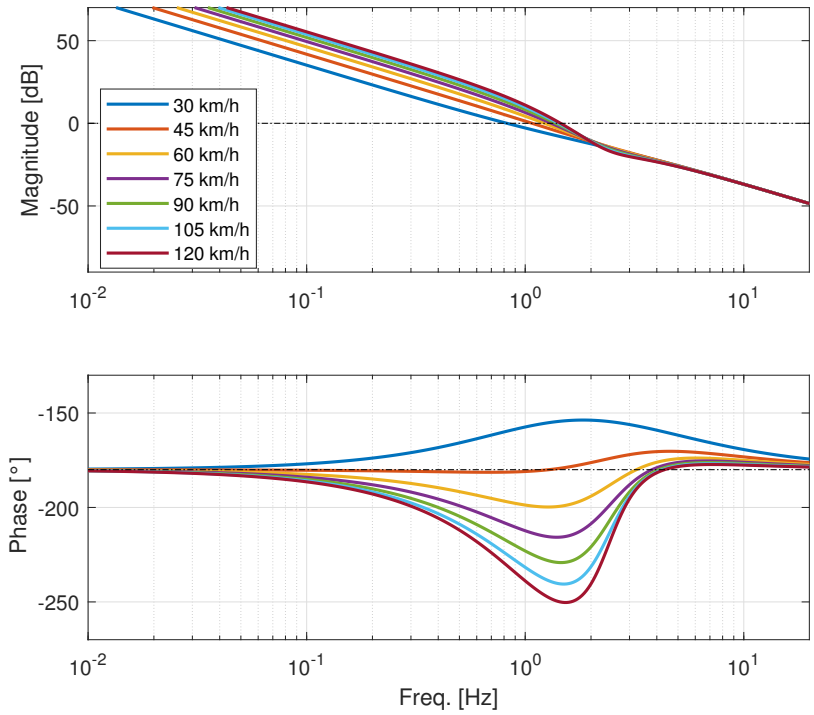

Figure 2.11: $G_{e_{cg}}$ at different velocities.

2.4.2 Dependence on the friction coefficient

Here it is highlighted the dependence of the vehicle model $G_{\delta_w \to ecg}(s)$ to the friction coefficient μ. This dependence is relevant in the non-nominal conditions where the road conditions are not as expected and the assumption of a friction

coefficient of $\mu = 1$ (dry asphalt) is not realistic. To complete this analysis it is considered that the cornering stiffness parameters C_f and C_r are proportionally dependent on the friction coefficient μ:

$$C_f \propto \mu \qquad C_r \propto \mu \tag{2.20}$$

Thus, the parameters C_f and C_r are accordingly scaled depending on the value of μ considered and a sensitivity analysis of the model to this parameter is reported in the bode plot in Figure 2.12. As μ decreases the bandwidth of the transfer function becomes lower too.

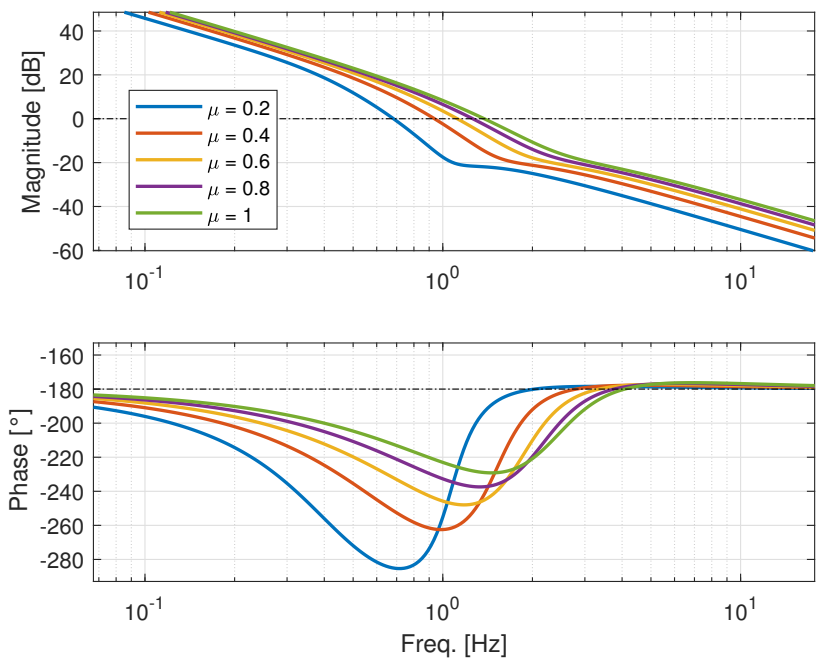

Figure 2.12: Sensitivity of $G_{\delta_w \to ecg}(s)$ to the friction coefficient μ.

2.5 Model of the vehicle in simulation

Since the physical vehicle was not available for experiments, in this thesis all the controllers have been validated on a simulator software: CarMaker.

CarMaker is a commercial software by IPG ([33]) which is capable of realistically and precisely simulate the handling characteristics of the vehicle as a response to different inputs, such as steering, accelerations and braking. This software is compatible with MATLAB Simulink, which is used to interact with the CarMaker environment. In Figure 2.13 is possible to see the interface of CarMaker and the 3D virtual world that shows the simulated experiment.

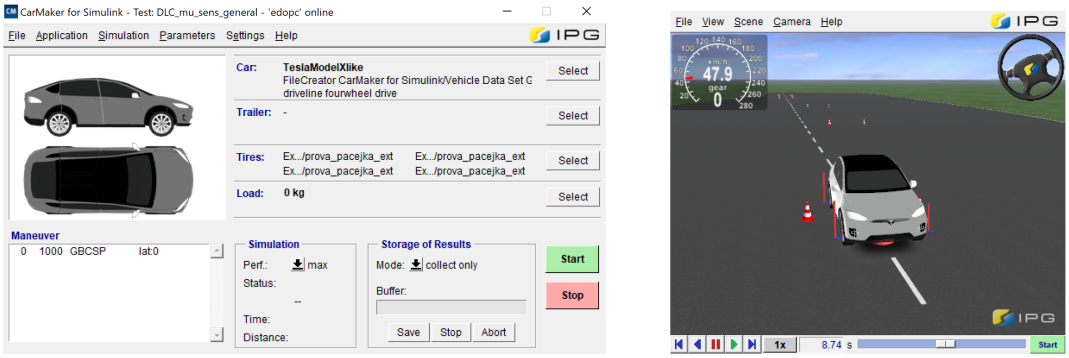

(a) GUI of CarMaker. (b) 3D simulation environment.

Figure 2.13: Some examples of views of CarMaker.

2.6 Definition of maneuvers

To assess the performance of the controllers and compare them, two main maneuvers are used: the Double Lane Change (DLC) and the Obstacle Avoidance (OA). These two maneuvers are defined in ISO 3888-1:2018 [34] and in ISO 3888-2:2011 [35]. These two standards don't define explicitly the path coordinates, but an area where the car must lie when performing the maneuver. The trajectories are characterized by quick variations of curvature that need high bandwidth control action to be accurately tracked.

2.6.1 Double Lane Change

The Double Lane Change (DLC) is a standard maneuver to evaluate the performances of the vehicle. The classic procedure of the test consists of a first straight sector where the throttle is released, a change on the left lane and a final change on the right lane. However, in this thesis, this maneuver is performed in a slightly different way: during the whole maneuver the velocity is kept constant by a simple longitudinal controller, therefore it is assumed the throttle is not released in the first sector. Note that this strategy allows testing the lateral controller in the case of both lateral and longitudinal controllers active, which is the nominal driving condition. Figure 2.14 and Table 2.2 report all the geometrical information about the DLC maneuver constraints.

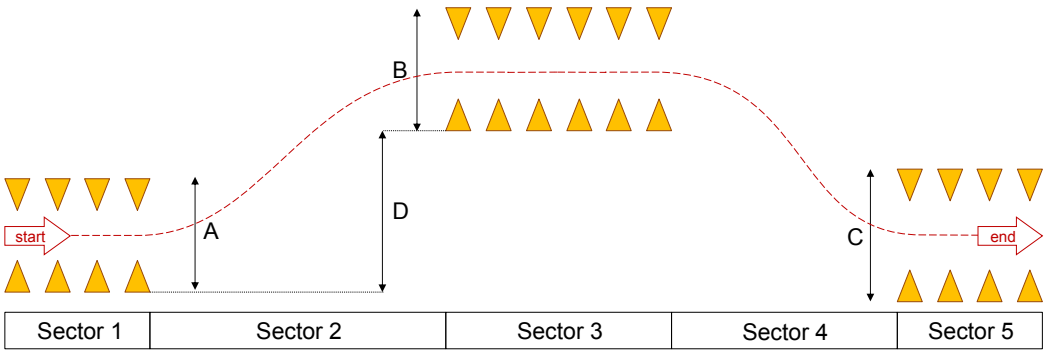

Figure 2.14: DLC maneuver scheme.

2.6.2 Obstacle Avoidance

The Obstacle Avoidance (OA) is an emergency maneuver, very common in safety tests. OA has two turns, one left and one right, but the spaces are more stringent with respect to the DLC. As for the DLC, the classic procedure of OA expects that the throttle is released at the beginning of the maneuver but, in this thesis work, the velocity is kept constant during the whole test. Figure 2.15 and Table 2.3 report all the geometrical information about the OA maneuver constraints.

Table 2.2: DLC geometrical dimensions.

Dimension name	**Formula**	**Length [m]**
Sector 1	-	15
Sector 2	-	30
Sector 3	-	25
Sector 4	-	25
Sector 5	-	15
A	$1.1 * w_v + 0.25\text{m}$	2.45
B	$1.2 * w_v + 0.25\text{m}$	2.65
C	$1.3 * w_v + 0.25\text{m}$	2.85
D	-	3.5

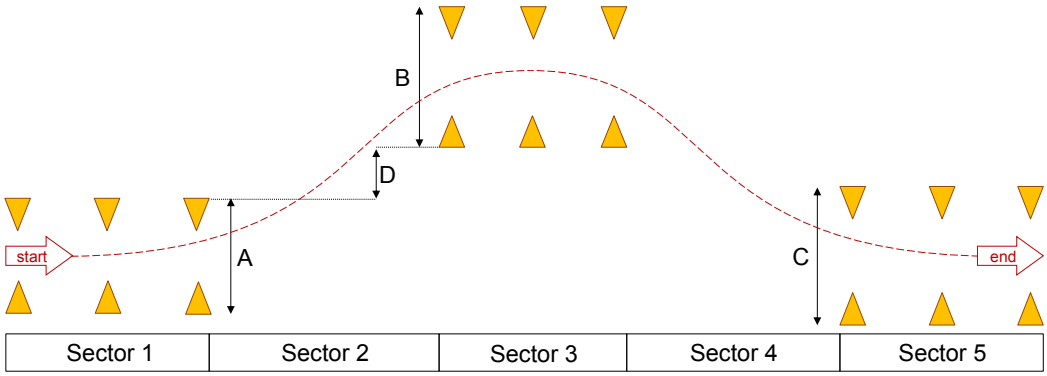

Figure 2.15: OA maneuver scheme.

Table 2.3: OA geometrical dimensions.

Dimension name	**Formula**	**Length [m]**
Sector 1	-	12
Sector 2	-	13.5
Sector 3	-	11
Sector 4	-	12.5
Sector 5	-	12
A	$1.1 * w_v + 0.25\text{m}$	2.45
B	$w_v + 1\text{m}$	3
C	-	3
D	-	1

Chapter 3

Control

In this chapter, the previously described models of the vehicle and the actuator will be used to design two lateral controllers. In the first section, the first controller is realized with classic loop-shaping techniques and it will serve as a benchmark. In the second section, a more sophisticated controller composed of three elements: a regulator that acts on the yaw-rate, a regulator that rejects the lateral error and a filter that exploits future information about the curvature. Both the controllers use the steering angle δ_w as the control variable and have the target curvature ρ_t as exogenous input.

3.1 Loop-shaping controller

Here it is presented a control strategy which mainly operates on the lateral error. The main control scheme is reported in Figure 3.1, where the models (already presented in Chapter 2) which characterize the scheme are: $G_{e_{cg}}(s)$, which is the transfer function between the steering angle δ_w and the lateral error e_{cg}; $G_\rho(s)$, which represents the dynamics between the curvature ρ_t and the lateral error e_{cg}; and the steering actuator one $G_{SW}(s)$ which is added in series with $G_{e_{cg}}(s)$ since its dynamics cannot be neglected. Finally the loop is closed with a

regulator, which is designed with loop-shaping techniques that will be discussed. After the tuning and the velocity scheduling of the regulator, an additional open-loop component will be considered to take in account the information on the curvature.

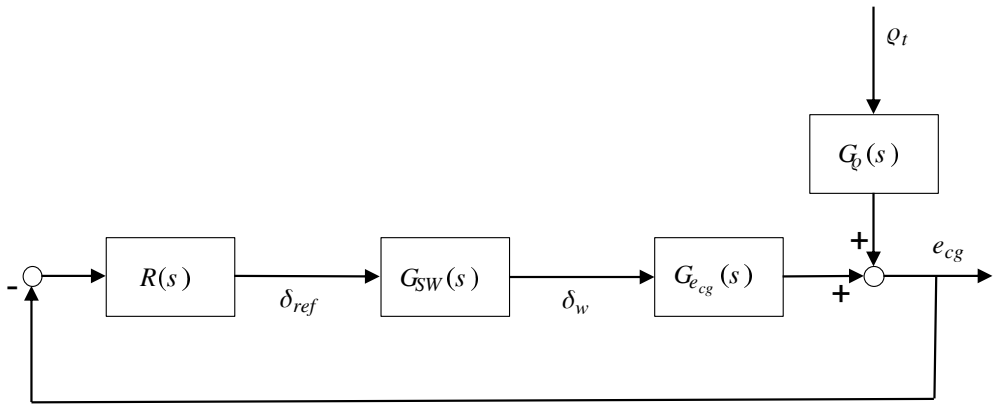

Figure 3.1: Loop-shaping Controller scheme.

3.1.1 Regulator structure and tuning

To understand which is the best regulator structure it is important to look at the loop transfer function:

$$G(s) = G_{SW}G_{e_{cg}} = G_{SW}\frac{V_x}{s^2}\frac{\tilde{N}(s)}{\tilde{D}(s)} \tag{3.1}$$

which represents the actuator model combined with the vehicle one and it is characterized by 2 zeros and 6 poles (2 of them are in zero). The regulator structure is chosen on the basis of the given specifications:

- the closed-loop system has to be stable;
- static precision: the system should be able to reject step disturbances of curvature;
- dynamic precision: obtain a bandwidth of at least 0.6 Hz and reduce the importance of the peak of resonance caused by the steering actuator.

To reject the disturbances an integrator must be included in the regulator structure, while to obtain a stable closed-loop system, two zeros should be added. Finally, a pole is needed to obtain a causal regulator and, moreover, this pole can be really helpful in reducing the effects of the steering actuator's resonance.

Hence the final structure of the regulator is:

$$R(s) = R^{\star}(s)\frac{\left(\frac{s}{2\pi f_z}+1\right)^2}{\frac{s}{2\pi f_p}+1} = \frac{k}{s}\frac{\left(\frac{s}{2\pi f_z}+1\right)^2}{\frac{s}{2\pi f_p}+1} \tag{3.2}$$

where f_z is the frequency of the free zeroes (which are chosen to be coincident for tuning simplicity), f_p is the frequency of the free pole and k is the gain. These three parameters are chosen to satisfy the dynamic specifications.

The tuning of these parameters was particularly challenging because the actuator delay and the vehicle dynamics cause a quick loss of phase after 1 Hz. Moreover the resonance peak has to be attenuated and this fact impose a limit to the increase in bandwidth. Considering these observations, the final parameters (Tab. 3.1) are tuned at 60 km/h such that a closed-loop bandwidth of 0.6 Hz and a phase margin of 40° is reached. In Fig. 3.2 the bode plot of the open-loop transfer function $L(s) = R(s)G(s)$ is reported. Note that the tuned combination of parameters makes possible to obtain a good trade-off between reducing the resonance peak (at 4 Hz) and increasing the bandwidth.

Table 3.1: Loop-shaping controller parameters.

k	$\mathbf{f_z}$	$\mathbf{f_p}$
$2 \cdot 10^{-4}$ rad/m	0.01 Hz	2 Hz

3.1.2 Sensitivity to velocity and scheduling

Since the vehicle model $G_{e_{cg}}(s)$ is dependent on the speed and the controller's parameters were tuned at 60 km/h, it is important to verify the behavior of the

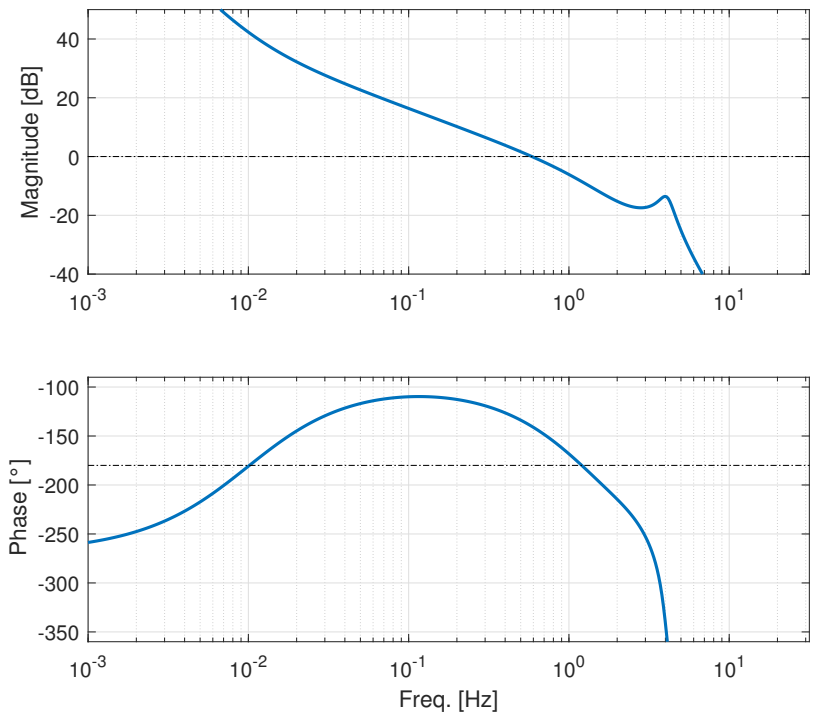

Figure 3.2: Bode plot of $L(s)$.

regulator at different velocities.

In Figure 3.3 a sensitivity of the open-loop transfer function $L(s)$ with respect to the velocity V_x is performed. From this analysis it is clear that for high velocities (more than 90 km/h) the phase margin is negative and thus, for the Bode criterion, the closed-loop system is not stable. Moreover the bandwidth varies a lot at different velocities.

Given the previous remarks, a scheduling in velocity of the controller is realized. The only element inside the open-loop function which changes depending on the velocity is $G_{e_{cg}}(s)$ and for this reason the following analysis is focused on this element.

To this scope, remember that in section 2.4.1 it was discussed the sensitivity of $G_{e_{cg}}(s)$ to the longitudinal velocity. The main difference is at low frequencies, therefore it is decided to use a multiplying factor $k_{sched}(V_x)$ to normalize $G_{e_{cg}}(s)$

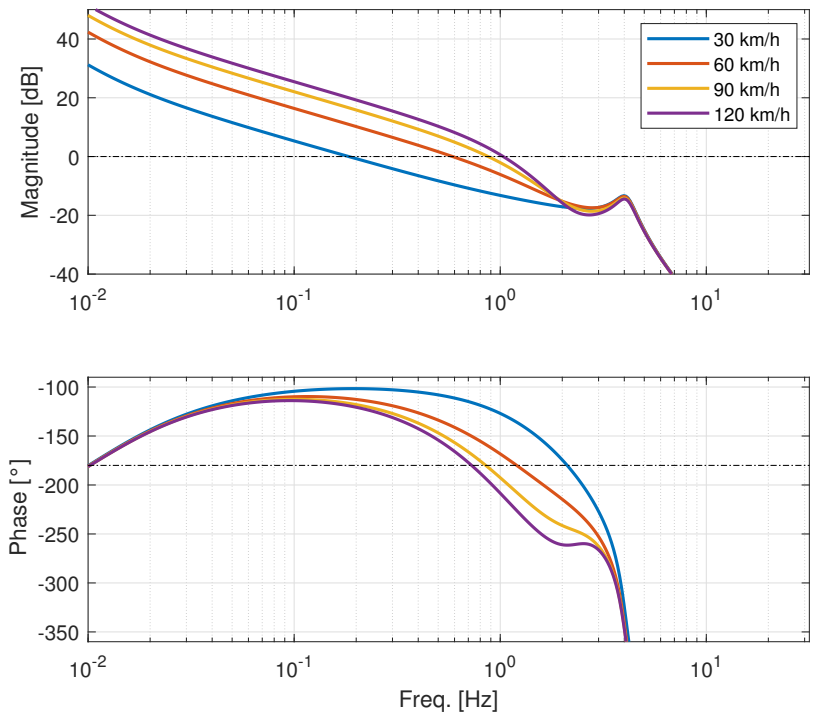

Figure 3.3: Sensitivity of $L(s)$ to longitudinal velocity.

in this range of frequencies at different velocities. The multiplying factor is set as:

$$
\begin{aligned}
k_{sched}(V_x) &= G_{e_{cg}}^{-1}(0) = \\
&= \frac{C_f C_r L^2 - m(C_f l_f - C_r l_r)V_x^2}{V_x^2 C_f C_r L} = \\
&= \frac{1}{V_x^2}\left(L - \left(\frac{m l_f}{C_r L} - \frac{m l_r}{C_f L}\right)V_x^2\right) = \\
&= \frac{1}{V_x^2}\left(L + \left(m\frac{C_f l_f - C_r l_r}{C_f C_r L}\right)V_x^2\right) = \\
&= \frac{L + K_{us}V_x^2}{V_x^2}
\end{aligned}
\tag{3.3}
$$

where K_{us} is the under-steering coefficient.

The normalization leaves untouched the tuned parameters f_z and f_p, but only

acts on the gain of the regulator, whose final expression is:

$$k(V_x) = k_{60} \frac{k_{sched}(V_x)}{k_{sched}(60 \text{ km/h})} \tag{3.4}$$

where k_{60} is the gain tuned at 60 km/h and already reported in Tab. 3.1.

In Figure 3.4 the open-loop function after the scheduling of velocity is shown. The difference in bandwidth at different velocities is now more limited (it is always around 0.6 Hz) and the closed-loop system is always stable, also at high speeds. The scheduling is applied for the velocities in the range between 40 km/h and 120 km/h.

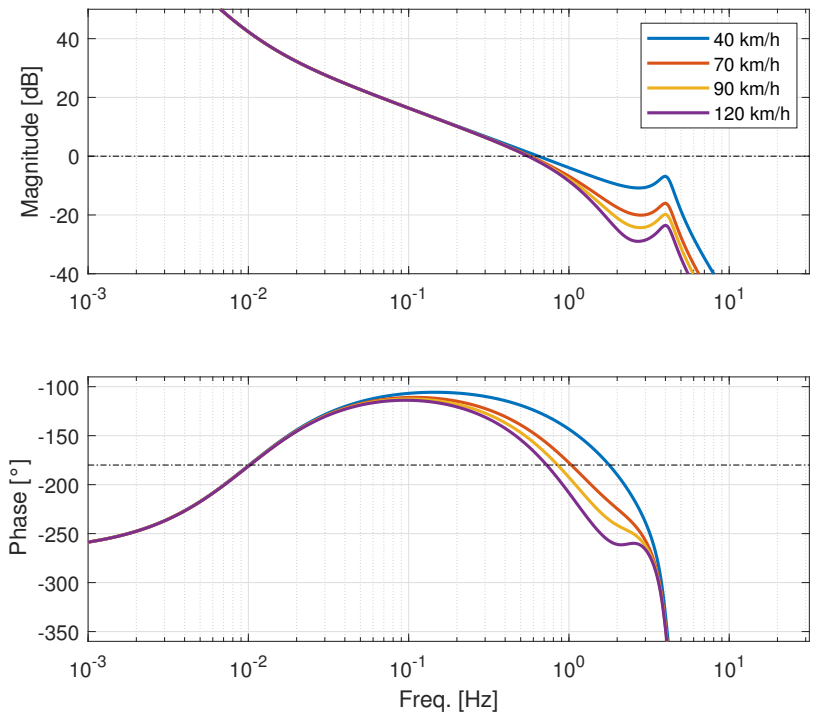

Figure 3.4: Bode plot of the open-loop transfer function $L(s)$ with the scheduling in velocity.

At this point the regulator is tuned and scheduled in velocity, however there is another information, additionally to the lateral error, that can be exploited to

improve the controller's performances: the road curvature. Hence a feed-forward compensation is realized.

3.1.3 Feed-forward compensation

As anticipated, the curvature is known and acts as a disturbance therefore we can use the theory on compensation of measurable disturbances (which is treated in many books, such as [36]) to realize a more performing control strategy. In particular a feed-forward component $C(s)$ based on the vehicle static model is used (Fig. 3.5). The main idea is that the curvature disturbance is exploited to anticipate the regulator and to directly give the compensating steering command. To cancel the effect of the curvature disturbance, $C(s)$ should be defined such that:

$$C(s)G_{SW}(s)G_{e_{cg}}(s) = -G_{\rho}(s) \tag{3.5}$$

If $C(s)$ was computed directly from the last expression, a not causal component would be obtained and it would be necessary to add high-frequency poles. Much more simply, $C(s)$ can be designed as a gain C_0 such that the equivalence 3.5 is true in static conditions; thus:

$$C(s) = C_0 = -(G_{SW}(0)G_{e_{cg}}(0))^{-1}G_{\rho}(0) = L + K_{us}V_x^2 \tag{3.6}$$

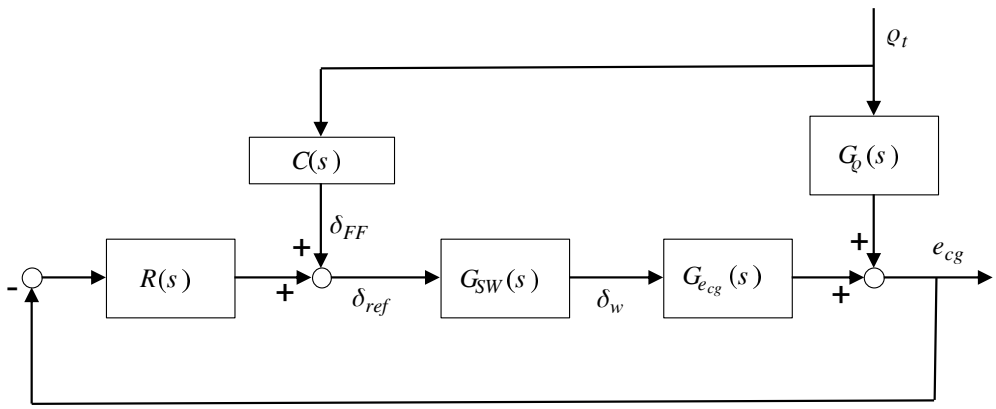

Figure 3.5: Complete controller scheme with the feed-forward action.

The feed-forward compensation directly reduce the lateral error, in fact without this compensation the lateral error increases and only after the regulator starts its correcting action. The main draw-back of the feed-forward component is that it is an open-loop component designed on the static model of the vehicle: this means that the performance of the feed-forward component depends on the quality of the model's description and therefore it lacks of robustness to changes of the model. Moreover only the current information of curvature is exploited. While in the next section, a more advanced controller is realized where the future information is used.

3.2 Curvature Preview Controller

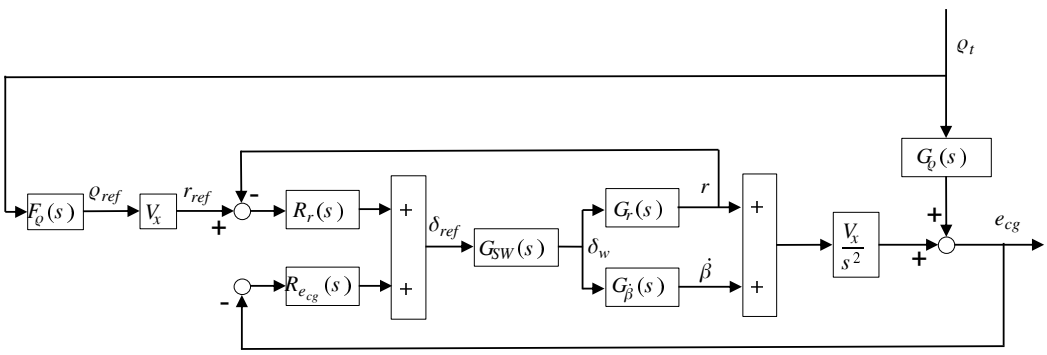

Figure 3.6: Complete controller scheme with the feed-forward action.

The control strategy here presented is taken from [16] and has a completely different structure with respect to the previous loop-shaping controller. The block diagram of the complete Curvature Preview Controller is shown in Figure 3.6, where $G_r(s)$ and $G_{\dot\beta}(s)$ are respectively the transfer function between the steering angle δ_w and the yaw rate r and the one between the δ_w and the derivative of the slip angle $\dot\beta$. Their expression, which can be derived by the single track model

(2.16), is:

$$\begin{aligned} G_r(s) =& \frac{C_f l_f m V_x^2 s + C_f C_r (l_r + l_f) V_x}{\tilde{D}(s)} \\ G_{\dot{\beta}}(s) =& \frac{C_f J_z V_x s^2 + (C_f C_r l_r^2 + C_f C_r l_f l_r - C_f l_f m V_x^2) s}{\tilde{D}(s)} \end{aligned} \tag{3.7}$$

with

$$\begin{aligned} \tilde{D}(s) =& J_z m V_x^2 s^2 + [(C_f + C_r) J_z + (C_f l_f^2 + C_r l_r^2) m] V_x s + \\ &+ C_f C_r (l_f + l_r)^2 + (C_r l_r - C_f l_f) m V_x^2 \end{aligned} \tag{3.8}$$

The controller is composed by two loops: one on the yaw rate r and one on the lateral error e_{cg}. Moreover a filter $F_\rho(s)$ is introduced and used to determine the reference of yaw rate. The following procedure has to be followed to properly design the control system:

1. design the yaw rate controller considering only the open-loop from the steering angle reference δ_{ref} to the yaw rate r;
2. design of the filter $F_\rho(s)$;
3. design of the lateral error controller considering also the yaw rate feedback.

3.2.1 Yaw-rate loop

In this phase the lateral error loop is not present and the filter $F_\rho(s)$ is set equal to 1, which means that the reference of yaw rate r_{ref} is equivalent to the reference curvature ρ_t times the speed V_x. $R_r(s)$ is chosen with a fixed structure:

$$R_r(s) = \frac{k_r}{s} \tag{3.9}$$

The parameter k_r should be tuned such that the bandwidth of the controlled system is higher than the expected excitation of the system. A way to determine the value of the maximum excitation in terms of bandwidth can be apply the Fourier transform to the reference yaw rate of the reference maneuvers discussed

in Section 2.6. In particular it is interesting to analyze the yaw rate reference at critical velocities. These yaw rate references are obtained by multiplying the curvature reference for the maximum speed at which the maneuver can be performed (the speed is supposed constant):

$$r_{ref}(t) = \rho_t(t) V_{x,max} \tag{3.10}$$

The maximum feasible velocity $V_{x,max}$ is found by looking at the maximum lateral acceleration (equal to the acceleration of gravity g) and assuming a friction coefficient $\mu = 1$:

$$V_{x,max} = \sqrt{\frac{\mu g}{\rho_{t,MAX}}} \tag{3.11}$$

where $\rho_{t,MAX}$ is the maximum curvature in absolute value.

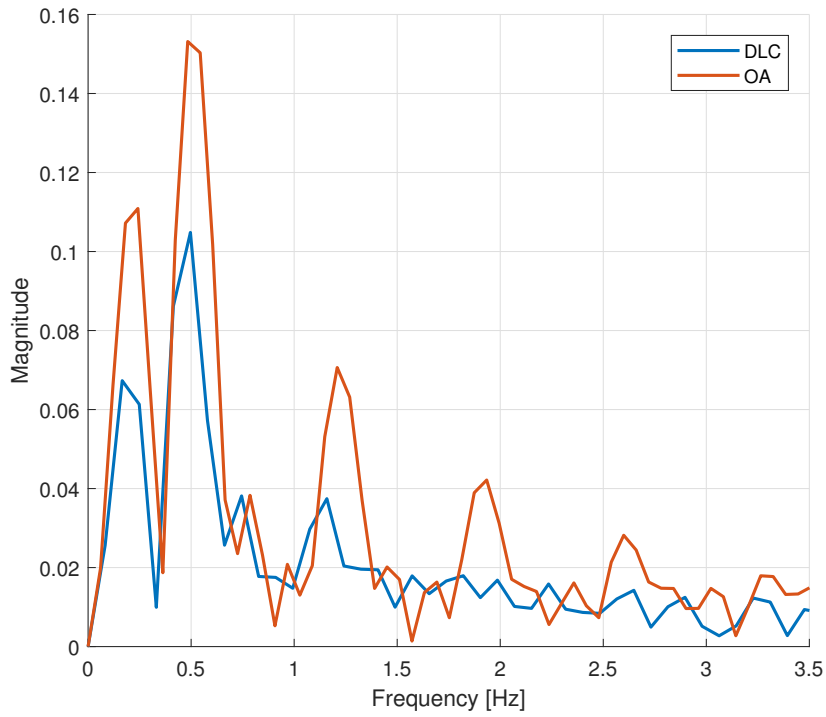

Figure 3.7: Fourier transforms of the reference maneuvers.

In Figure 3.7 the spectra of the critical, but still feasible, DLC and OA maneuvers are reported. DLC and OA maneuvers were respectively performed at

$V_{x,max}^{DLC} = 61.1$ km/h and $V_{x,max}^{OA} = 30.3$ km/h. The main frequency components are lower than 1 Hz, hence there is no need for the yaw rate controller to have a bandwidth higher than this value.

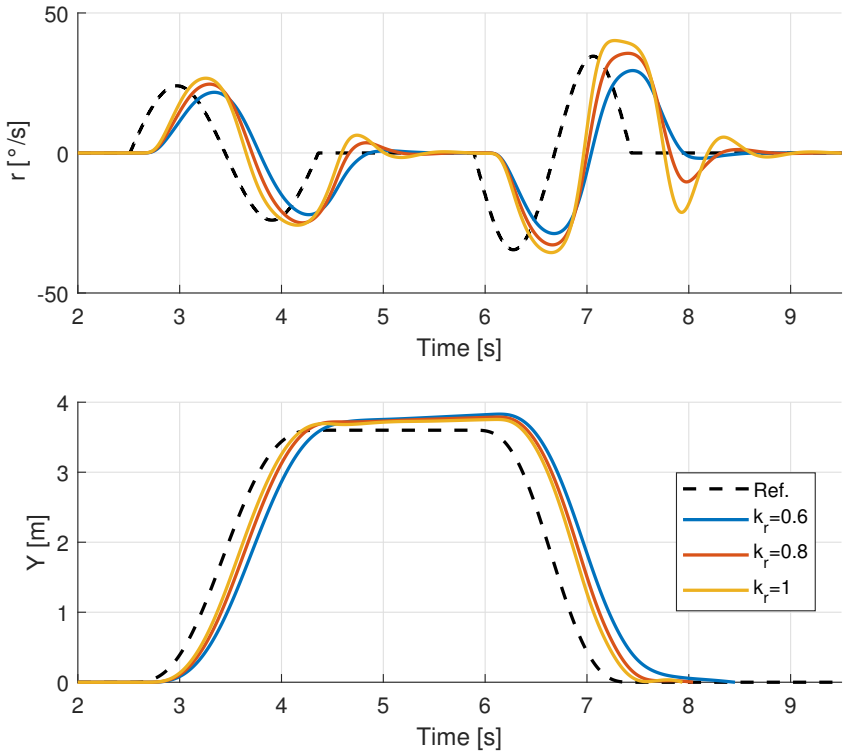

Figure 3.8: k_r sensitivity analysis on the DLC maneuver.

Some simulations can help to understand how the yaw rate controller has effect on the trajectory accomplished by the vehicle. Figure 3.8 shows a sensitivity analysis to the gain k_r, when the controller is fed with a DLC reference maneuver at 60 km/h. It is interesting to notice that, for certain values of the gain (around $k_r = 0.7 \div 1.1$), the obtained lateral displacement is very similar to the reference one but shifted in time. To explain this behavior the expression of the lateral error is considered:

$$e_{cg} = G_{\rho_{ref} \to e_{cg}} \rho_{ref} - G_{\rho} \rho_t \tag{3.12}$$

where:

$$G_{\rho_{ref}\to e_{cg}}(s) = \frac{R_r(s)G_{SW}(s)(G_r(s)+G_{\dot{\beta}}(s))}{1+R_r(s)G_{SW}(s)G_r(s)}\frac{V_x^2}{s^2} \tag{3.13}$$

Since in this case $\rho_{ref} = \rho_t$, the perfect tracking ($e_{cg} = 0$) is obtained when $G_{\rho_{ref}\to e_{cg}} = G_\rho$. By comparing $G_\rho(s)$ with $G_{\rho_{ref}\to e_{cg}}(s)$ using different k_r (Figure 3.9) it can be noticed that the two transfer functions match up to a certain value of frequency, while the phases diverge at much lower values of frequency. This clarify why there was a time-shift of the lateral displacement with respect to the reference. To achieve the requested bandwidth of 1 Hz it is enough to choose the value $k_r = 0.8$ since it allows to have $G_{\rho_{ref}\to e_{cg}} = G_\rho$ up to this frequency.

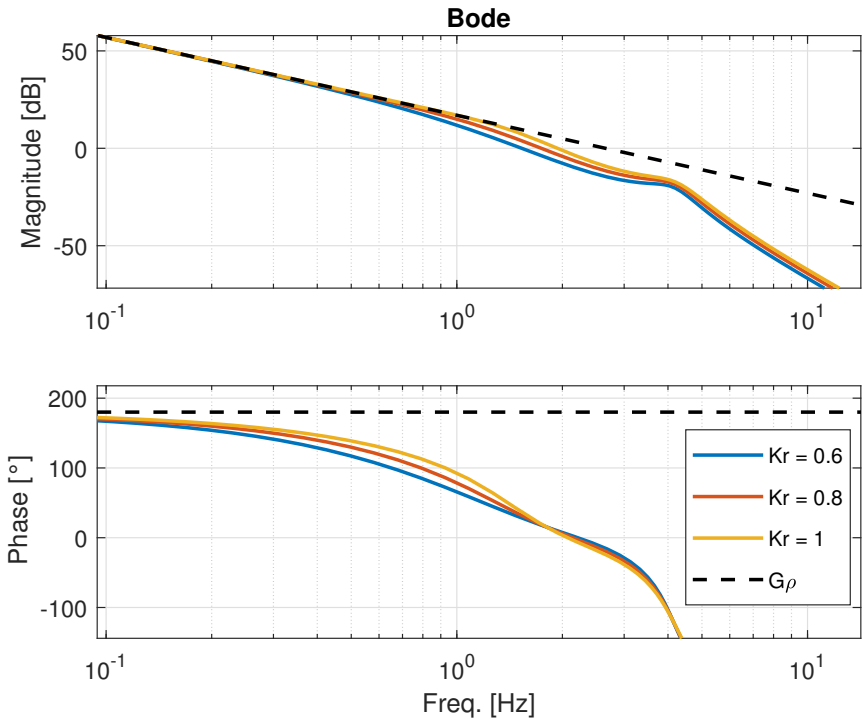

Figure 3.9: Sensitivity to k_r of $G_{\rho_{ref}\to e_{cg}}(s)$ at 60 km/h.

3.2.2 Curvature filter

As seen the yaw rate controller is not able to cancel completely the lateral error in the frequency range of interest. The scope of the filter $F_\rho(s)$ is to overcome

this limitation. The expression of the error 3.12 can be updated as:

$$e_{cg} = G_{\rho_{ref} \to e_{cg}} F_\rho(s)\rho_t - G_\rho \rho_t \tag{3.14}$$

from which it can be derived:

$$F_\rho(s) = \frac{G_\rho(s)}{G_{\rho_{ref} \to e_{cg}}(s)} \tag{3.15}$$

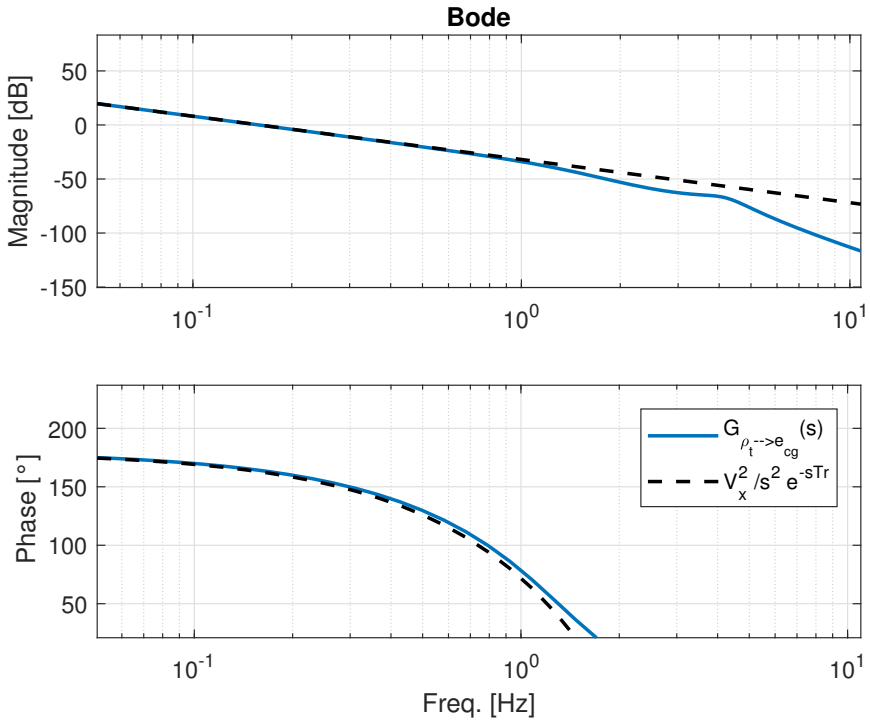

Figure 3.10: Approximation of the transfer function $G_{\rho_{ref} \to e_{cg}}(s)$.

Based on the considerations done in the section of the yaw rate controller, it is possible to describe the model $G_{\rho_{ref} \to e_{cg}}(s)$ as equal to $G_\rho(s)$ with a time delay:

$$G_{\rho_{ref} \to e_{cg}}(s) \approx \tilde{G}_{\rho_{ref} \to e_{cg}}(s) = \frac{V_x^2}{s^2} e^{-sT_r} \tag{3.16}$$

where T_r is a parameter that will be tuned. Figure 3.10 shows a comparison between the model $G_{\rho_{ref} \to e_{cg}}(s)$ and the approximated function $\frac{V_x^2}{s^2} e^{-sT_r}$: there is a good match up to the requested bandwidth of 1 Hz. Therefore by using this

approximation in 3.15:

$$F_\rho(s) = e^{sT_r} \tag{3.17}$$

which correspond to a time-advance of T_r seconds. Filtering the reference curvature with a time advance means that a future value of curvature must be given as reference to the yaw rate control. This is not a problem because the curvature trajectory is known.

The parameter T_r is tuned in such a way that the time delay in the path tracking is canceled. The identified value of the time advance is $T_r = 0.21$ s. In Figure 3.11 it is shown that by giving the curvature preview (the light blue line) as reference it is possible to improve the matching between the yaw rate trajectory accomplished by the vehicle (the blue line) and the target yaw rate trajectory (the black line). The time advance is such that the yaw rate response is almost perfectly aligned with the trajectory one.

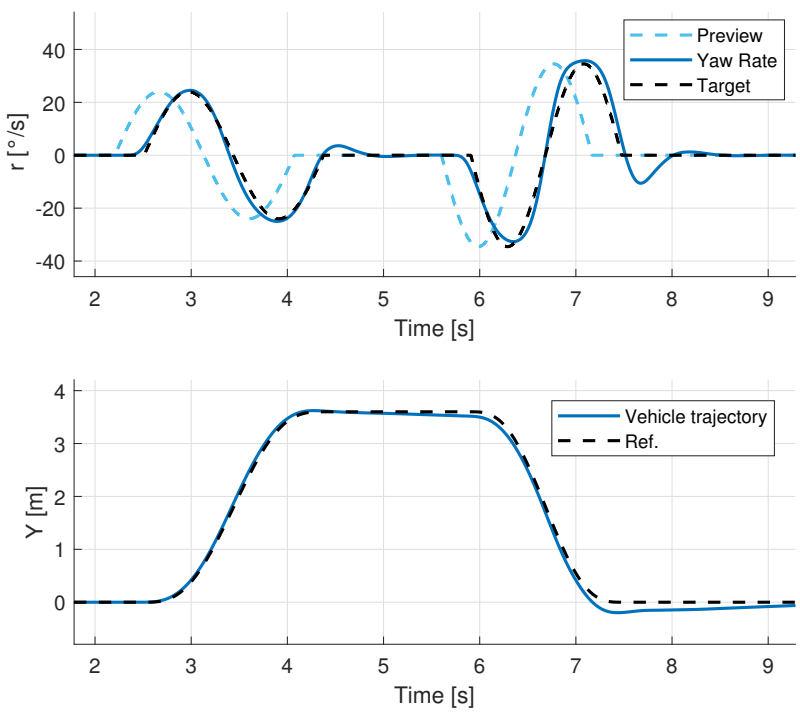

Figure 3.11: Effect of the curvature reference filtering.

The yaw rate controller proved to be able to accurately track high dynamics maneuvers such as DLC at critical velocities. The main drawback of this approach is that it doesn't consider the actual position of the vehicle with respect to the reference path, but only its variability in terms of curvature. The presence of uncertainties in the model and the approximations made in the design of $F_\rho(s)$ would cause the drifting of the vehicle with respect to the reference path. The error which will gradually build up is:

$$\tilde{e}_{cg}(t) = (F_\rho(s)G_{\rho_{ref}\to e_{cg}}(s) - G\rho(s))\rho_t(t) \tag{3.18}$$

For this reason an additional loop on the lateral error which deals with low frequency dynamics is designed.

3.2.3 Lateral Error loop

To design the lateral error control loop, a new contribute to the control action has to be add. It will be now composed by a term obtained from the yaw rate regulator and a term given by the lateral error regulator:

$$\delta_{ref}(t) = \delta_r(t) + \delta_e(t) \tag{3.19}$$

To design the new regulator the yaw rate feedback has to be included. ρ_{ref} and ρ_t are the two inputs and, in particular, the sum of these two terms, multiplied respectively by $G_{\delta_e\to e_{cg}}(s)$ and $G_\rho(s)$, is the residual error $\tilde{e}_{cg}$ of the yaw rate control system. $\tilde{e}_{cg}$ can be seen as a disturbance that the lateral error regulator has to reject. Thus the system can be treated as a SISO system.

The rearranged block diagram in Figure 3.12 makes easier to understand the design of the lateral error regulator $R_e(s)$. The transfer function $G_{\delta_e\to e_{cg}}(s)$, which relates the steering angle asked by the lateral error regulator and the lateral error, is defined as:

$$G_{\delta_e\to e_{cg}}(s) = \frac{G_{SW}(s)(G_r(s) + G_{\dot{\beta}}(s))}{1 + R_r(s)G_{SW}(s)G_r(s)}\frac{V_x^2}{s^2} \tag{3.20}$$

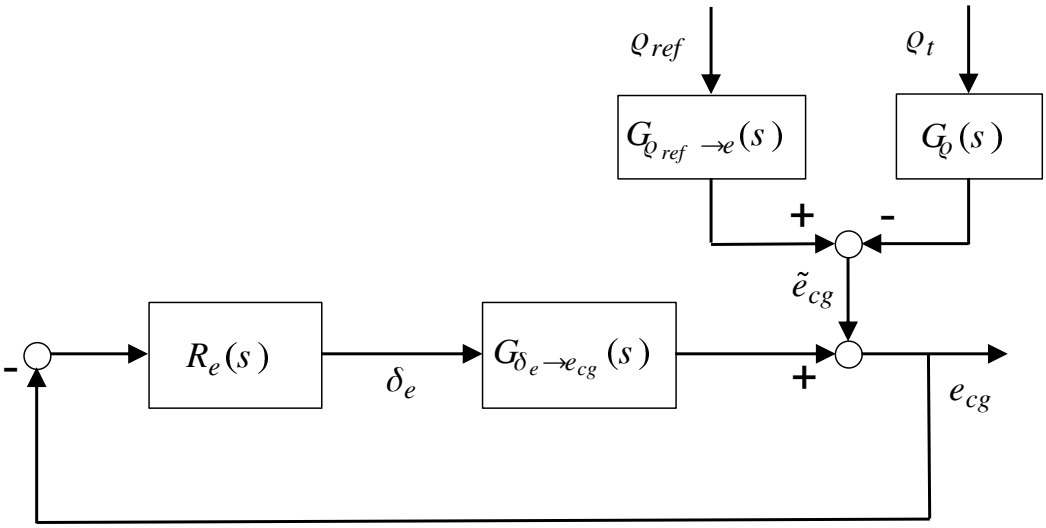

Figure 3.12: Rearranged control scheme for the design of $R_e(s)$.

The controller $R_e(s)$ will be designed using standard loop-shaping techniques, fixing a specific speed. Then a velocity scheduling described by [16] is presented and finally a more fine scheduling is reported.

The regulator is designed with the following structure:

$$R_e(s) = \frac{k_e}{s} \frac{\left(\frac{s}{2\pi f_{ez}} + 1\right)^2}{\frac{s}{2\pi f_{ep}} + 1} \tag{3.21}$$

with the following characteristics:

- an integrator to achieve a null lateral error at steady-state;
- a couple of coincident zeros to increase the phase between 0.1 Hz and 1 Hz;
- a pole to have a causal transfer function.

Fixing the longitudinal speed at 90 km/h the parameters are tuned so that a bandwidth of 0.3 Hz and phase margin of 85° are reached. The chosen parameters are reported in Table 3.2.

Table 3.2: Lateral error regulator's parameters.

$\mathbf{k_e}$	$\mathbf{f_{ez}}$	$\mathbf{f_{ep}}$
0.0045	0.05 Hz	0.3 Hz

In Figure 3.13 it is reported the sensitivity analysis to different speeds of the open loop function and it is noticeable a wide variability in the bandwidth. To solve this problem a possible approach can be the one followed by [16], where only the gain k_e is scheduled.

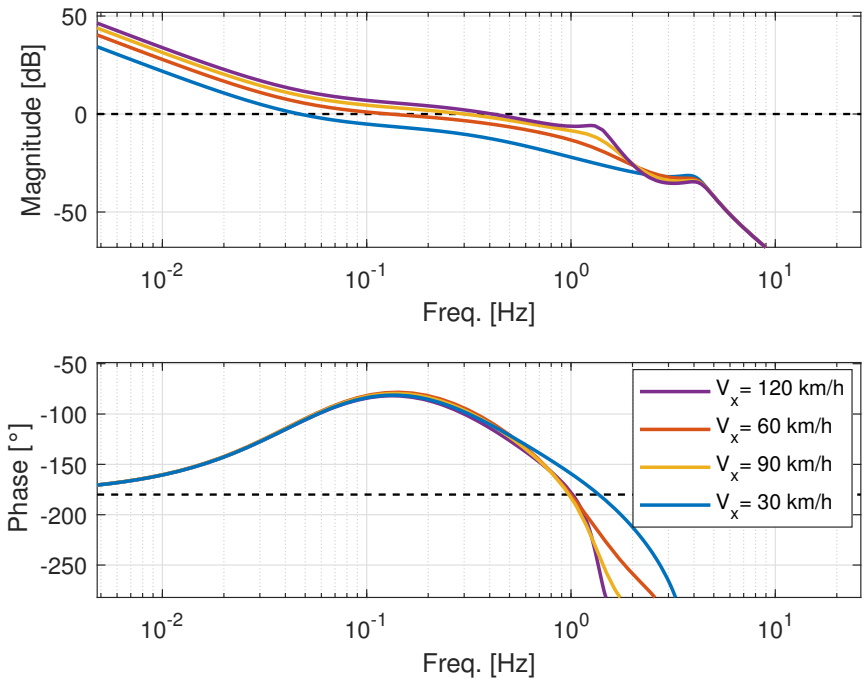

Figure 3.13: Sensitivity to V_x of the open-loop function $R_e(s)G_{\delta_e \to e_{cg}}(s)$.

It is possible to notice that, for low frequencies, $G_{\delta_e \to e_{cg}}(s)$ corresponds to an integrator and a proportional term:

$$G_{\delta_e \to e_{cg}}(s) \approx \frac{G_{\delta_e \to e_{cg}}(0)}{s} = \frac{V_x}{k_r s} \tag{3.22}$$

Interestingly, the gain only depends on the coefficient k_r of the yaw rate controller and is directly proportional to the longitudinal speed V_x.

After these considerations, the expression of the gain of the lateral error regulator can be changed with:

$$k_e(V_x) = k_{e,90}\frac{90 \text{ km/h}}{V_x} \tag{3.23}$$

where $k_{e,90}$ is the gain previously tuned at 90 km/h and reported in Tab. 3.2.

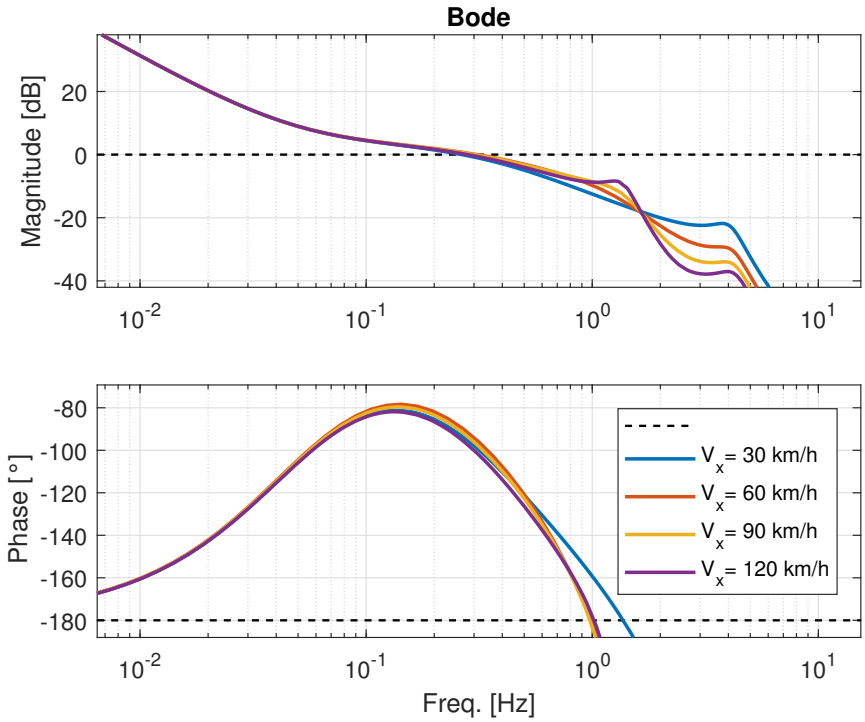

Figure 3.14: Sensitivity to V_x of $R_e(s)G_{\delta_e \to e_{cg}}(s)$ with gain scheduling.

This solution makes possible to realize a controller which have a fixed bandwidth of about 0.3 Hz at all the speeds (Figure 3.14).

3.3 Conclusions

In this chapter there were presented two different strategies to control the lateral dynamics of the vehicle. The design of them is based on the linear single

track model and the considered control input is the steering angle.

The Loop-shaping controller is realized with a single regulator designed to reject the curvature disturbance. This regulator has one integrator, two zeros and one pole and it is tuned to have a bandwidth of 0.6 Hz. A velocity scheduling is also implemented in the range between 40 km/h and 120 km/h . Moreover, the control action of the regulator is supported by the presence of a model based feed-forward component.

The second controller realized is the Curvature Preview controller which in the following chapter will be proven to have better results. This control strategy is obtained by designing one curvature filter and two regulators, one closes a loop on the yaw rate and one on the lateral error. These two regulators are tuned separately and, in particular, the one that controls the yaw rate has a bandwidth of 1 Hz, while the other one of 0.3 Hz. The latter is also scheduled in velocity to guarantee this bandwidth in a range between 30 km/h and 120 km/h. Finally, the curvature filter $F_\rho(s)$, which is what mainly distinguishes this controller from the first one, is designed as a time advance that allows to have future information on the curvature and therefore permit an anticipation of the control action.

Chapter 4

Controllers results

In this chapter, the controllers are tested and the results will be analyzed. The first section deals with the comparison between the Curvature Preview controller and the Loop-shaping controller, which is used as a benchmark, and it will be proven the superiority of the first controller. The comparison is done on the Double Lane Change and the Obstacle Avoidance maneuvers. In the second section, it will be discussed the problem of the robustness of the controllers to grip changes: some simulations of a Double Lane Change on a road with lower friction will be shown.

4.1 Comparison of the controllers

This section is devoted to a comparison between the two controllers and the indexes which are going to be used to evaluate the different performance are:

- the maximum lateral error, which gives an insight into the path tracking quality in the most critical instants;

- the root mean squared error gives, instead, information about the general behavior during the whole test;

- the maximum lateral acceleration, which is useful to assess how aggressive the maneuver is;

- the maximum slip angle that is another interesting parameter to evaluate the aggressiveness;

The maneuvers used for the comparison are the Double Lane Change and the Obstacle Avoidance, which were already introduced in section 2.6and which are both characterized by quick variations in the curvature.

All the simulations will be performed on the software CarMaker. During the maneuvers, the speed is regulated and to achieve this task a simple velocity control strategy is used. With this intention, it is considered a PI regulator, tuned such that the bandwidth of the longitudinal dynamics is lower than 0.1 Hz (in this way any interference with the lateral controllers is avoided).

4.1.1 Double Lane Change

The Double Lane Change is an aggressive maneuver but it can also be performed at relatively high velocity. In particular, the car was able to successfully execute the DLC up to a maximum velocity of 90 km/h. Thus, the range between 30 km/h and 90 km/h is the one studied.

In Figure 4.1 a comparison between the indexes of the two controllers is reported and every result will be now commented. Focusing the attention on the lateral error, it is possible to notice that up to 60 km/h both the controllers have good performances and the error is always limited to 0.1 m or even less. For higher velocities, the Loop-shaping controller shows a great increase in the lateral error, indeed at 80 km/h and 90 km/h goes out of scale reaching respectively 1.10 m and 1.33 m. Differently, the Curvature Preview controller keeps the error always lower than 0.10 m, except at 90 km/h for which the error slightly increases (only 0.17 m).

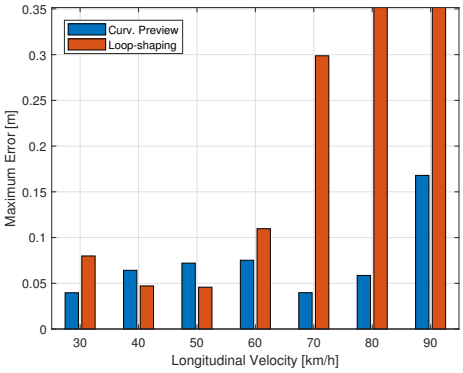

(a) Maximum lateral error.

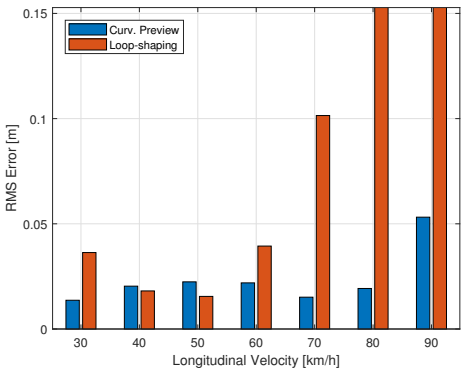

(b) RMS error.

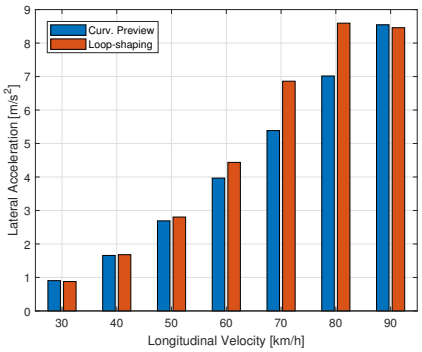

(c) Maximum lateral acceleration.

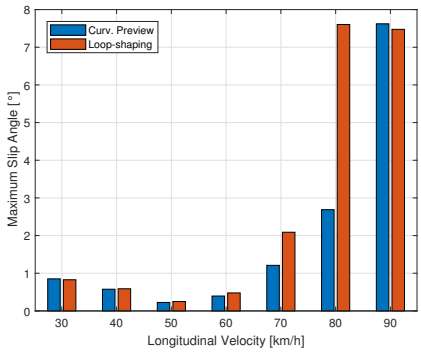

(d) Maximum slip angle.

Figure 4.1: Comparison between Curvature Preview and Loop-shaping controllers. DLC.

Similar considerations can be made also for the RMS error and this means that the tracking problems of the Loop-shaping controller at high speeds are not isolated to some critical points, but are present in substantial sections of the maneuver.

The maximum lateral accelerations at the highest velocities are reaching the physical kinetic limit of the vehicle. Moreover for speeds higher than 70 km/h the accelerations are greater than $0.4g$ and the slip angle β reaches not negligible values; these two conditions go against the assumptions made during the derivation of the single-track model, which means that the vehicle dynamics is not perfectly

described in these cases. However, the Curvature Preview Controller is demonstrating still a good tracking: this can be translated into good robustness of the controller. To better understand the differences between the two controllers few simulations are reported now, in particular, the simulations at 30 km/h, 60 km/h and 90 km/h are showed.

In Figure 4.2 it is presented the simulation at 30 km/h. It represents a simple maneuver, with accelerations lower than 1 m/s^2 and small slip angles. It is quite clear that both the controllers manage to track correctly the given trajectory. The Loop-shaping controller, coherently with what was said before, has a slightly minor acceleration, but there are few oscillations, which are absent in the Curvature Preview.

The simulation at 60 km/h (Fig. 4.3) is characterized by greater accelerations (however not higher than 5 m/s^2) and the slip angle is still very low, actually comparable to the maneuver at 30 km/h. Looking to the lateral displacement and the steering angle, it is noticeable that the Loop-shaping controller starts to steer after a certain amount of time and this because only the current information of the curvature is exploited, differently from the Curvature Preview controller, which exploits future information.

At 90 km/h (Figure 4.4) the differences between the two controllers are much more evident. As anticipated, only the Curvature Preview has a good tracking of the reference maneuver. The accelerations almost reach the maximum lateral acceleration of $\mu g = 9.81$ m/s^2 (red dashed line), however the accelerations of the Curvature Preview follow better the expected kinematic acceleration (black dashed line), which was computed considering the velocity and the curvature reference as $a_{kin}(t) = V_{x,ref}^2(t)\rho_{ref}(t)$.

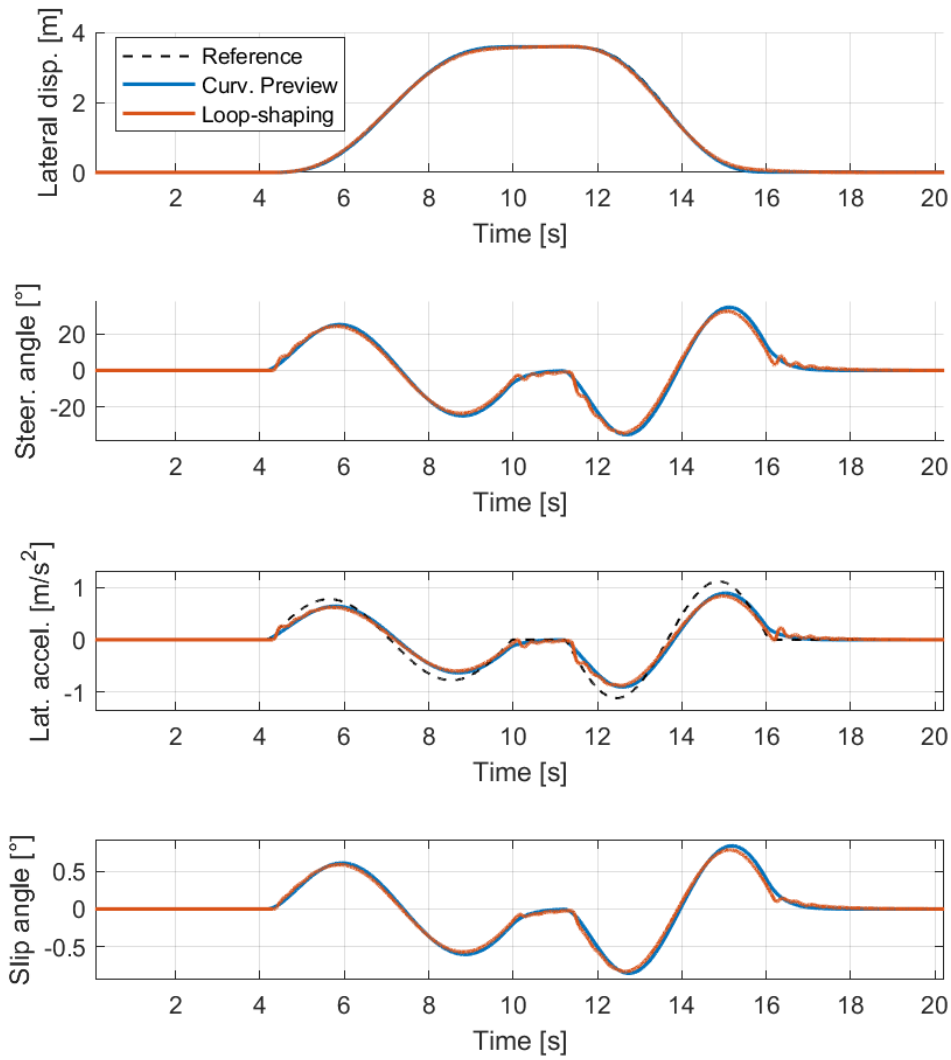

Figure 4.2: Simulation on DLC at 30 km/h.

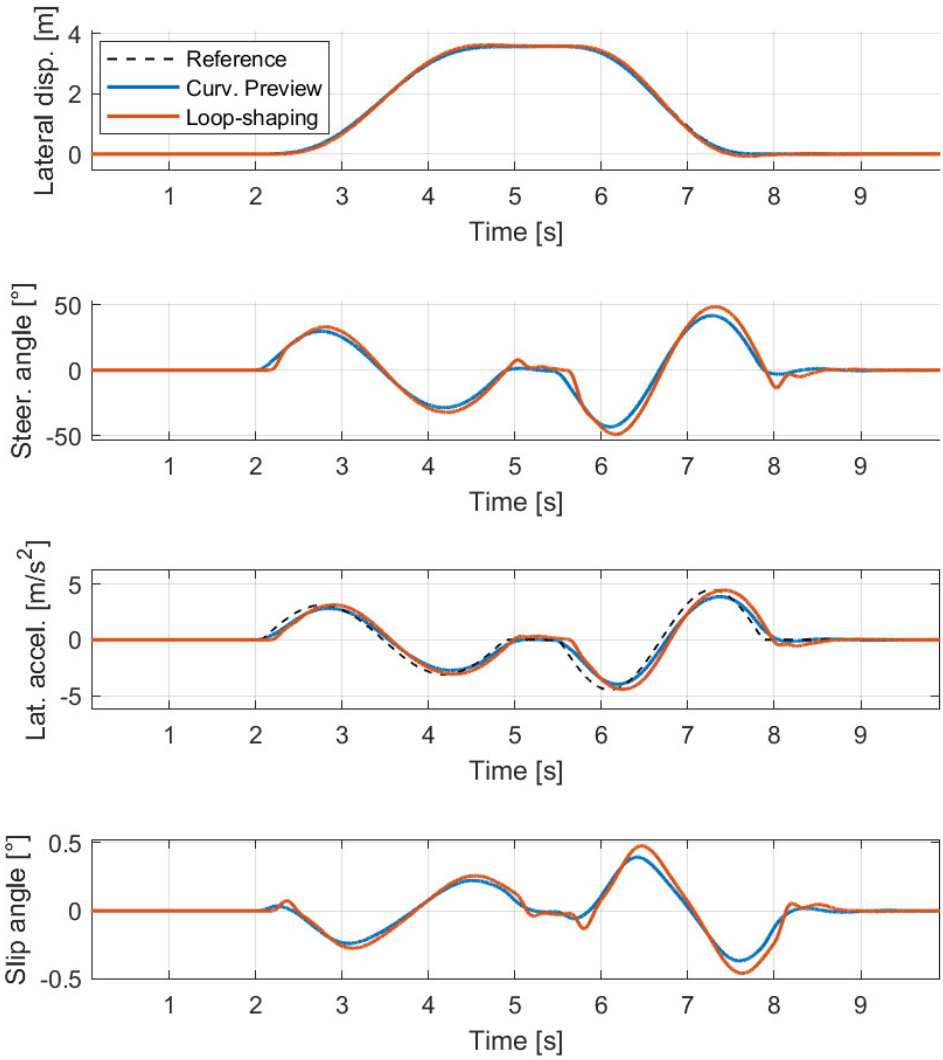

Figure 4.3: Simulation on DLC at 60 km/h.

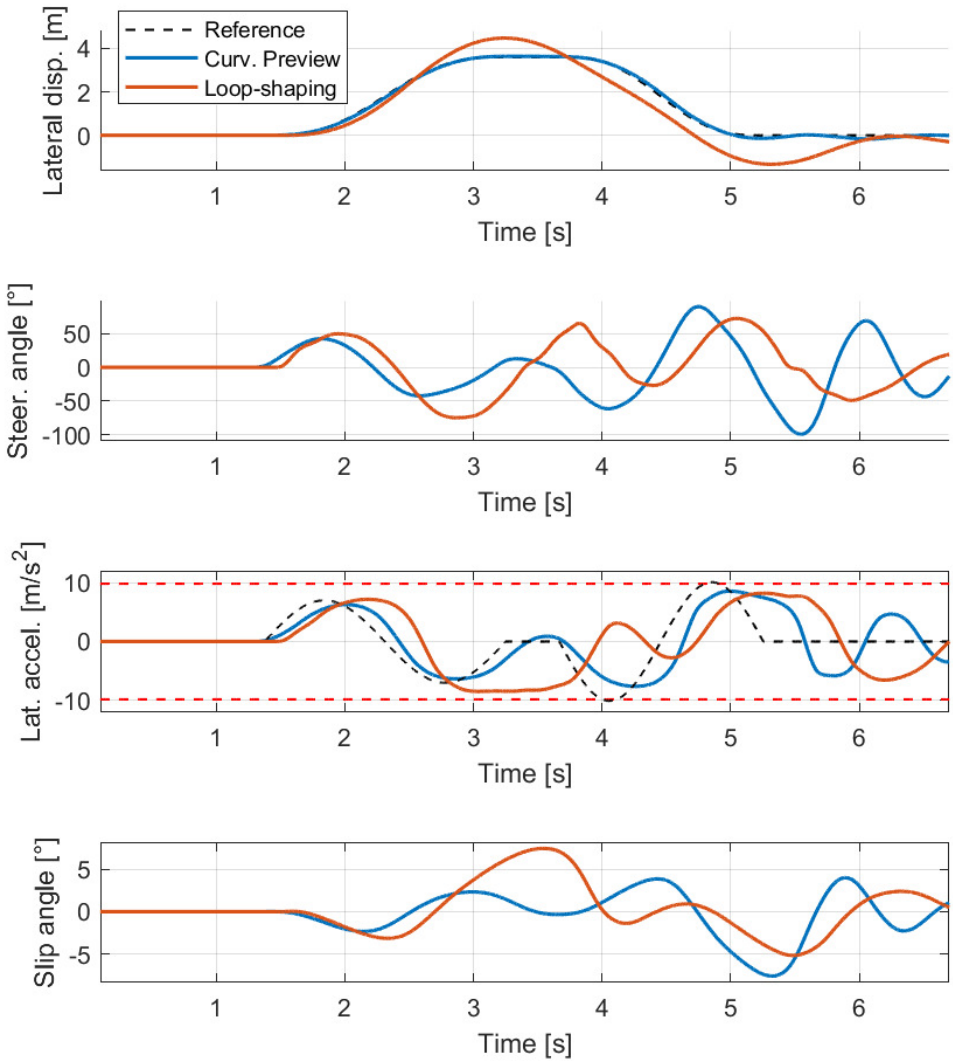

Figure 4.4: Simulation on DLC at 90 km/h.

4.1.2 Obstacle Avoidance

The Obstacle Avoidance is a maneuver much more exciting than the DLC because the change of lanes happens in less space. Thus, the range of speed considered here is 30 km/h to 60 km/h since the best controller can perform successfully the OA at these speeds. Moreover, it will be explained why the OA at 60 km/h is not a feasible maneuver and how, nevertheless, the Curvature Preview can pass the test.

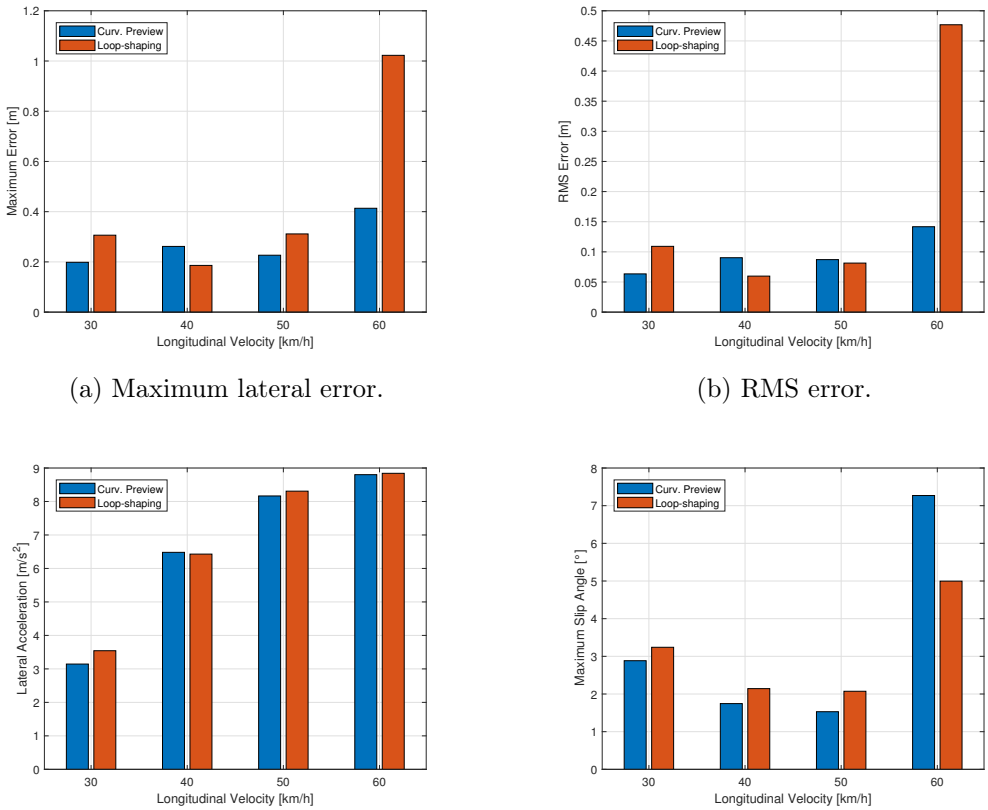

(a) Maximum lateral error.

(b) RMS error.

(c) Maximum lateral acceleration.

(d) Maximum slip angle.

Figure 4.5: Comparison between Curvature Preview and Loop-shaping controllers. OA.

Looking at Figure 4.5, it can be perceived the higher difficulty of this maneuver: the lateral error is slightly greater with respect to the DLC's ones. However,

it is less than 0.30 m for the Loop-shaping controller and less than 0.25 m in the Curvature Preview one. At 60 km/h the errors are larger, 1 m for the first and 0.4 m for the Curvature Preview. This is normal because the trajectory is unfeasible and it is not physically possible for the controllers to cancel the lateral error. Nevertheless, the Curvature Preview can limit the error to only 0.4 m and the Obstacle Avoidance test is even passed successfully. The RMS error shows that on average the error in the Curvature Preview is limited to be less than 0.15 m, which is reasonably a good result for such exciting maneuvers.

Considerations analogous to the DLC maneuver indexes can be done for the lateral accelerations and the slip angles: for greater speeds (50 km/h and 60 km/h) the accelerations and the slip angles reach high values. Still, the vehicle is kept stable.

Now the case at 60 km/h (Figure 4.6) is analyzed and its non-feasibility will be proven. This can be understood by looking at the graph of the accelerations: the kinetic acceleration is higher than the maximum one and when this happens the controller cannot track the reference. Note that both the controllers have high lateral accelerations and slip angles. They both manage to keep the control of the vehicle, however, the Curvature Preview obtains an error that is less than half with respect to the Loop-shaping controller.

After this analysis of the results, it can be concluded that using the Curvature Preview controller can give better performances with respect to the Loop-shaping one in particular in critical maneuvers. For this reason in the rest of the work the Curvature Preview controller is used as the main control strategy.

4.2 Sensitivity to the friction coefficient

To test the robustness of the Curvature Preview controller to different road conditions, a sensitivity analysis varying the friction coefficient μ is conducted. The interesting cases are the ones that already have a high lateral acceleration in

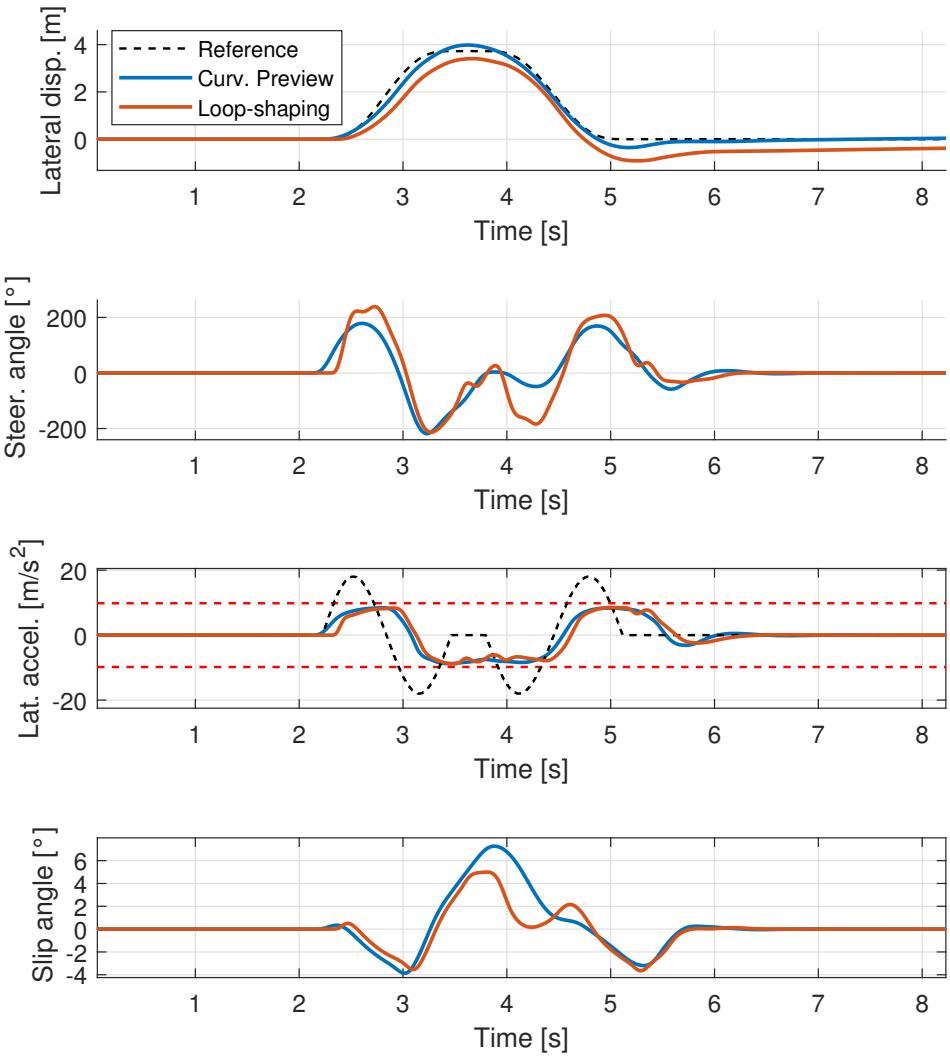

Figure 4.6: Simulation on OA at 60 km/h.

nominal conditions ($\mu = 1$, which is generically the friction coefficient considered for asphalt dry roads); for this reason, the Double Lane Change at 90 km/h is used. The tested friction coefficients μ are 0.5 and 0.8 and a comparison with the performances of $\mu = 1$ is reported in Figure 4.7. It can be noticed that for $\mu = 0.8$ the great part of the maneuver is tracked but the controller fails to stabilize the vehicle after the second lane change. Differently, for $\mu = 0.5$ the maneuver is not correctly performed and neither the first lane change is correctly completed.

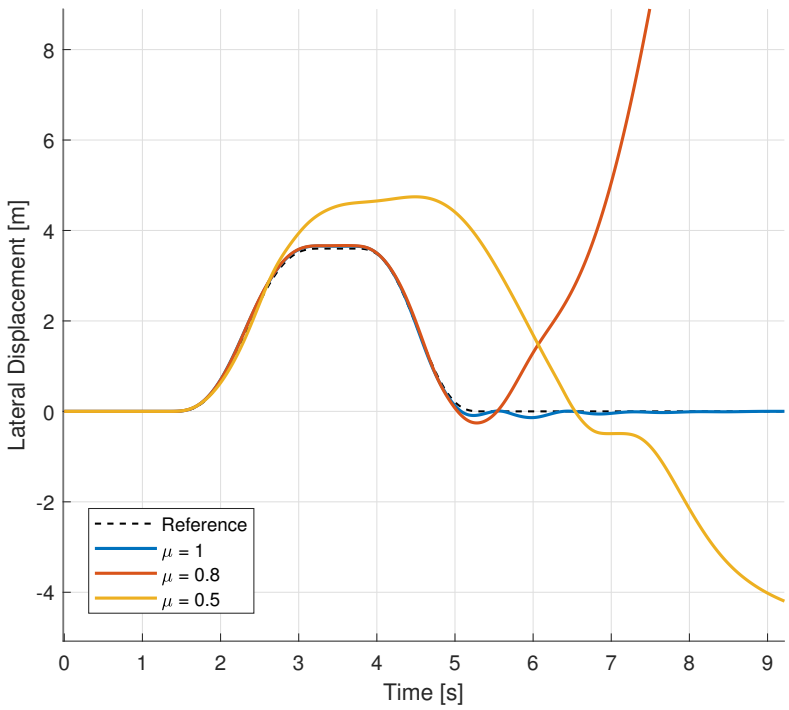

Figure 4.7: Sensitivity of the tracking performances to different friction coefficients.

This behavior can be understood by looking at Figures 4.8 and 4.9, which respectively report the simulations with $\mu = 0.8$ and $\mu = 0.5$. The decrease of the friction coefficient limits the maximum lateral acceleration (red dashed line) and the more the requested kinetic acceleration exceeds the limits the more the slip angle increases. This causes the tires to saturate and the steering control input

becomes ineffective (as proved in [37]). Therefore, in this situation, the controller counter-acts increasing the steering input and the slip increases enormously: the vehicle starts to drift without control and the path followed by the car diverges from the reference one.

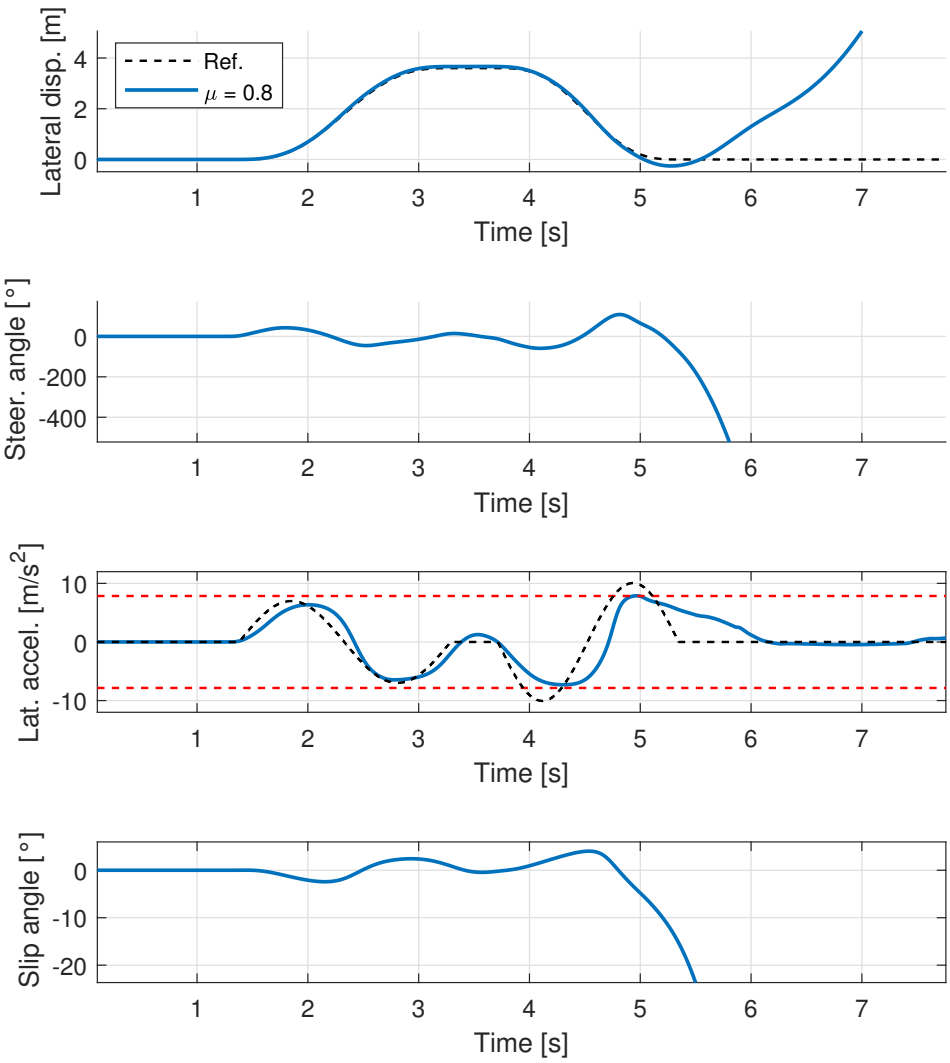

Figure 4.8: DLC simulation using a friction coefficient of $\mu = 0.8$.

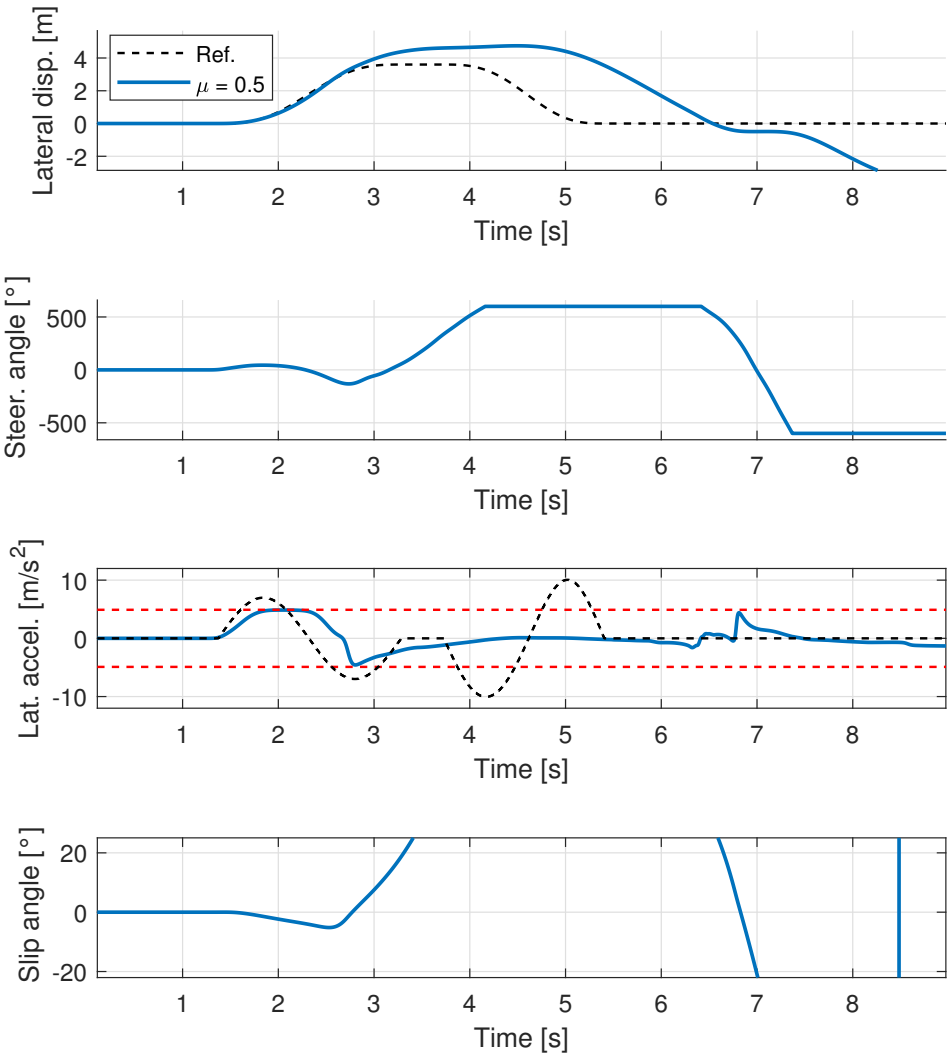

Figure 4.9: DLC simulation using a friction coefficient of $\mu = 0.5$.

In the case with $\mu = 0.8$ the great part of the maneuver is feasible, however after the double lane change (at about 5 s) the lateral acceleration is at the maximum, the steering angle is increasing in value and the vehicle becomes unstable, as is possible to see from the high slip angle values. While for $\mu = 0.5$ the acceleration exceeds the limit as soon as the car starts to steer and this causes the controller to rapidly lose the control of the vehicle.

It is clear the need for the implementation of a strategy to deal with non-nominal friction coefficients. The controller is demonstrated to be not robust to friction changes and for this reason, a solution will be proposed addressing the problem to the trajectory generation task.

4.3 Conclusions

In this chapter it was proved the superiority of the Curvature Preview controller over the Loop-shaping one: both the Double Lane Change and the Obstacle Avoidance maneuvers are successfully tracked in a range of velocity respectively between 30 km/h and 90 km/h and between 30 km/h and 50 km/h. The maximum lateral errors are of 0.17 m for the DLC at 90 km/h and of 0.23 m for the OA at 50 km/h, by considering only the feasible maneuvers.

At high velocities, it is shown that the non-linear area of the tires is reached, due to the high accelerations. Nonetheless, the Curvature Preview can exploit the maximal lateral forces of the tire and successfully track the maneuver. Remarkably this controller demonstrates to be robust also to maneuvers which demand slightly unfeasible accelerations such as the OA at 60 km/h, where however the maneuver is tracked with an error of only 0.41 m.

On the other hand, if the demanded acceleration highly exceeds the limits of the maximum lateral accelerations, such in the case of low friction conditions, the controller is not able anymore to act and the vehicle could become unstable. These considerations highlight the importance of feeding the controller with a

feasible trajectory; this means not only take account of the speed of the maneuver but also evaluate the road conditions and coherently design a path reference.

Chapter 5

Trajectory generation

In this chapter, another fundamental aspect of the autonomous driving systems is studied: the trajectory generation. In the first section, an algorithm to produce a feasible path made of sinusoidal waves will be presented. In the second section, an extension of this algorithm to deal with unexpected changes in the road conditions will be proposed. In these situations, the controller is already fed with a trajectory, but the sudden change in the friction coefficient makes it unfeasible. Hence, it will be explained how to replan a new feasible reference when needed. In the third section, this replanning strategy will be validated in simulation and its limitations will be discussed.

5.1 Sinusoidal lane-change maneuver

In driving situations and particularly in emergency ones, it is very common to execute lane-changes: the Double Lane Change and the Obstacle Avoidance maneuvers, which were used to compare the controllers, are two classic examples of these situations. It is important to have an effective algorithm to generate such a maneuver and, for this reason, the lane-change algorithm used in [16] is now introduced. When planning a path there are some constraints to satisfy:

- assuming constant speed V_x, there is a kinematic limit on the maximum curvature due to the maximum steering angle:

$$\rho_{max} = \frac{1}{\sqrt{l_r^2 + \frac{L^2}{\tan(\delta_{max})}}} \tag{5.1}$$

- assuming constant speed V_x and friction coefficient μ, there is a dynamic limit on the maximum curvature due to the maximum acceleration:

$$A_{y,max} = \mu g = \rho_{max} V_x^2 \implies \rho_{max} = \frac{\mu g}{V_x^2} \tag{5.2}$$

- the frequency of the curvature reference f_{ref} should not exceed the controller bandwidth ($f_{band} = 1$ Hz) and, moreover, it should be chosen taking into account the friction coefficient:

$$f_{ref} = \min(f_{band}, f_{MAX}(\mu)) \tag{5.3}$$

  where $f_{MAX}(\mu)$ is the maximum allowed frequency to keep the vehicle stable at a certain friction coefficient. An explanation of this will be given after (Section 5.1.1).

Note that the kinematic limitation is relevant only at very low-speed driving (e.g. parking maneuvers), which are outside the scope of this work. Differently, the dynamic limitation is much more important because it represents a real limitation at high speeds.

The main idea behind the proposed trajectory is to exploit the maximum curvature available to perform the lane change as fast as possible. At the same time, the frequency components of the path should be limited therefore it is chosen to use sinusoidal arcs with the correct frequency to link reference pieces of constant maximum curvature. This sinusoidal trajectory should appear similar to the one in Figure 5.1.

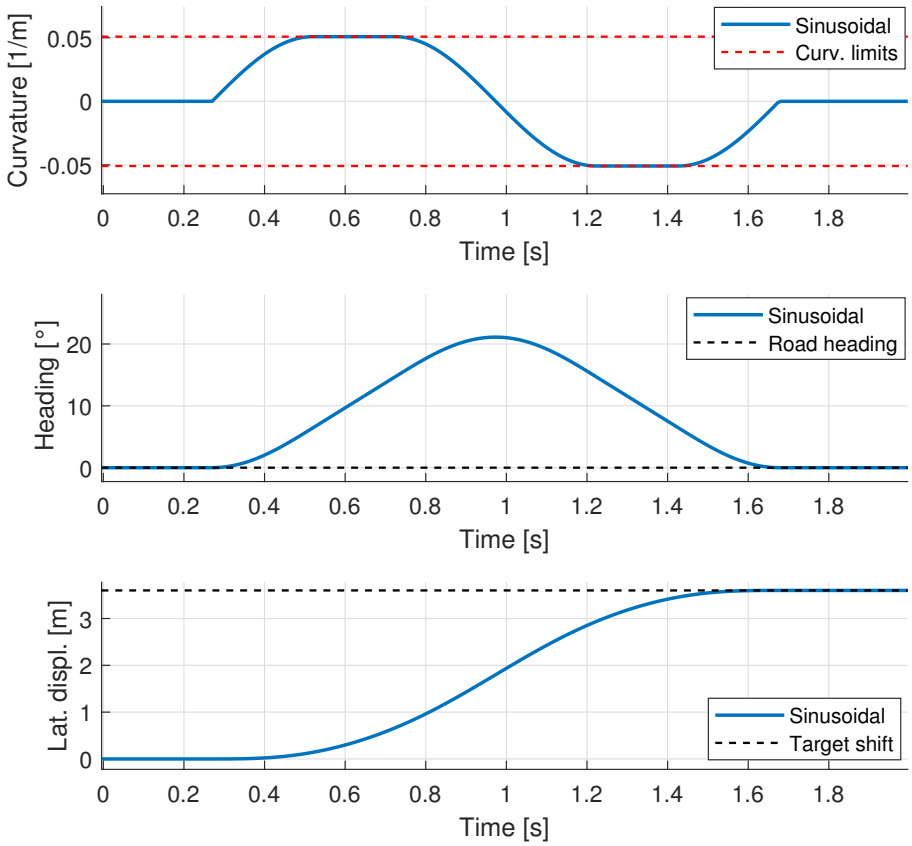

Figure 5.1: Example of sinusoidal lane change maneuver at 50 km/h.

The equation which defines this reference of curvature is:

$$\rho(t) = \begin{cases} \rho_1 \sin\left(\frac{2\pi}{T_c} t\right) & \text{if } \left[0, \frac{T_c}{4}\right] \\ \rho_1 & \text{if } \left[\frac{T_c}{4}, \frac{T_c}{4} + T_{12}\right] \\ \rho_1 \cos\left(\frac{2\pi}{T_c}\left(t - \frac{T_c}{4} - T_{12}\right)\right) & \text{if } \left[\frac{T_c}{4} + T_{12}, \frac{T_c}{2} + T_{12}\right] \\ \rho_2 \sin\left(\frac{2\pi}{T_c}\left(t - \frac{T_c}{2} - T_{12}\right)\right) & \text{if } \left[\frac{T_c}{2} + T_{12}, \frac{3T_c}{4} + T_{12}\right] \\ \rho_2 & \text{if } \left[\frac{3T_c}{4} + T_{12}, \frac{3T_c}{4} + T_{12} + T_{22}\right] \\ \rho_2 \cos\left(\frac{2\pi}{T_c}\left(t - \frac{3T_c}{4} - T_{12} - T_{22}\right)\right) & \text{if } \left[\frac{3T_c}{4} + T_{12} + T_{22}, T_c + T_{12} + T_{22}\right] \end{cases} \tag{5.4}$$

where T_c is the period of the sinusoid and it is chosen as $T_c = 1/f_{ref}$; T_{12} and T_{22} are the interval of time during which the curvature is kept constant with values of, respectively, ρ_1 and ρ_2. The generic sinusoidal lane change is composed of two pieces with constant curvature and other sinusoidal parts that link them. However if the maximum curvature is large enough it is possible that these limits are not reached, hence the curvature won't have constant parts (i.e. T_{12} and T_{22} are equal to 0 s) and it will be composed of just two pure sinusoidal waves with amplitudes of ρ_1 and ρ_2.

To correctly build the trajectory given by 5.4, it is important to impose some constraints such that the unknowns T_{12}, T_{22}, ρ_1 and ρ_2 can be determined. In fact, to complete a lane change, the generated trajectory needs to obtain the target shift y_{shift} and the final heading error of 0°. The lateral displacement and of the heading are given by:

$$\begin{aligned} \psi(t) &= \int_0^{t_{end}} V\rho(t)dt \\ y(t) &= \int_0^{t_{end}} V\psi(t)dt \end{aligned} \tag{5.5}$$

where t_{end} is the total time to complete the lane change, in particular: $t_{end} = T_{12} + T_{22} + T_c$. Solving these integrals and by imposing the final conditions, the following equations are obtained:

$$\begin{aligned} \psi(t_{end}) &= V\left(\rho_1\frac{T_c}{\pi} + \rho_1 T_{12} + \rho_2\frac{T_c}{\pi} + \rho_2 T_{22}\right) = 0 \\ y(t_{end}) &= V^2\left(\frac{T_c^2}{4\pi}(\rho_1 - \rho_2) + \frac{1}{2}(\rho_1 T_{12}^2 - \rho_2 T_{22}^2) + T_c\left(\frac{1}{4} + \frac{1}{2\pi}\right)(\rho_1 T_{12} - \rho_2 T_{22})\right) \\ &= y_{shift} \end{aligned} \tag{5.6}$$

These conditions are specific for a lane change on a straight road; however this can be also extended to cornering situations by coherently changing the values of y_{shift} and by taking a $\psi(t_{end}) \neq 0°$, equal to the final road orientation after the corner.

Notice that in the system 5.6 there are four unknowns, i.e. ρ_1, ρ_2, T_{12} and T_{22}, but only two equations, therefore there is not an unique solution. Solve a system like this requires to use an optimization strategy that is computationally expensive. However, it is possible to set some cases which will make two unknowns dependent on the others. In this way, the system has a unique solution which can be solved analytically, without great computational effort. To do so, a first solution is obtained by setting T_{12} and T_{22} to 0 s. This allows solving the system because only ρ_1 and ρ_2 are unknown and a trajectory made of pure sinusoidal waves is obtained. By comparing this solution with the limits of maximum curvature $\pm\rho_{max}$ (defined by the kinematic and dynamic limits in 5.1 and 5.2), three different cases are possible:

1. The maximum curvature ρ_{max} is not reached. Thus, the trajectory made of pure sinusoidal waves can be used as the final one;

2. The maximum curvature ρ_{max} is exceeded. Therefore, the pure sinusoidal curvature is not feasible and it is necessary to limit $\rho_1 = \pm\rho_{max}$ and $\rho_2 = \mp\rho_{max}$, where the sign is decided based on the lateral shift such as that $\text{sign}(\rho_1) = \text{sign}(y_{shift})$. The signs of ρ_1 and ρ_2 are chosen always opposite to avoid cusps, which are characterized by frequency components higher than the control bandwidth. The only free variables will be T_{12} and T_{22};

3. In case of cornering situations the waves can have amplitudes ρ_1 and ρ_2 that are not equal in absolute value. It can happen that only one of them exceeds the maximum curvature ρ_{max}. In such case the exceeding amplitude ρ_1 (or ρ_2) must be limited to ρ_{max}, while T_{22} (or T_{12}) can be set to 0 s. The remaining variables are the two unknowns.

The algorithm here described allows computing efficiently a lane change that respects the limits on maximum curvature and on a given frequency.

5.1.1 Choice of f_{ref}

As anticipated, in this section it is explained how to choose the correct value of the frequency of the sinusoidal reference. This frequency should be not higher than the controller bandwidth but also a more stringent constraint given by the friction coefficient μ needs to be considered.

To explain this, remember that in Section 2.4.2 it was addressed the problem of the dependence of the vehicle transfer function on the friction coefficient. These variations to the vehicle model were not considered during the design of the controller and, as it was proved in the simulations (Section 4.2), the controller is not able to track the maneuvers on low friction roads. To better understand this problem, it is reported a sensitivity analysis of the closed loop transfer function $G_{\rho_{ref} \to e_{cg}}(s)$ to the parameter μ in Figure 5.2.

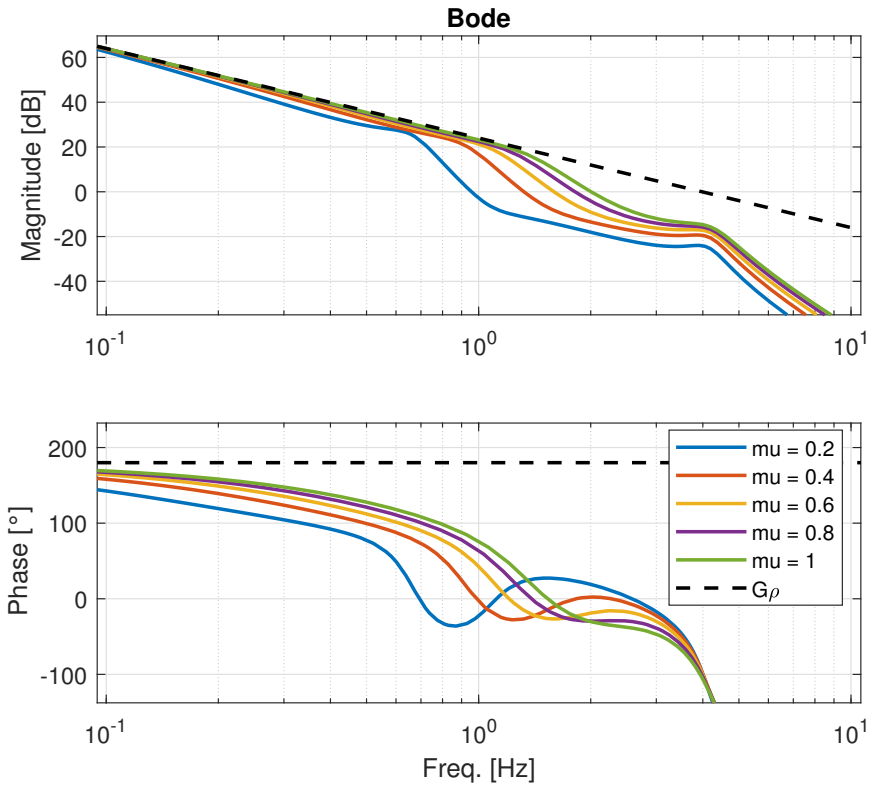

Figure 5.2: Sensitivity of $G_{\rho_{ref} \to e_{cg}}(s)$ to μ.

During the design of the controller (in nominal conditions with $\mu = 1$) the transfer function $G_{\rho_{ref} \to e_{cg}}(s)$ was assumed approximated to G_ρ up to a frequency of 1 Hz. For lower frictions it is possible that this approximation is not valid anymore. To correct this problem it is considered a frequency $f_{MAX}(\mu)$ which represents the frequency for which the approximation is still valid in the different conditions. A map of such a parameter is reported in Figure 5.3. As the friction coefficient decreases a lower frequency will be used and a milder path will be realized.

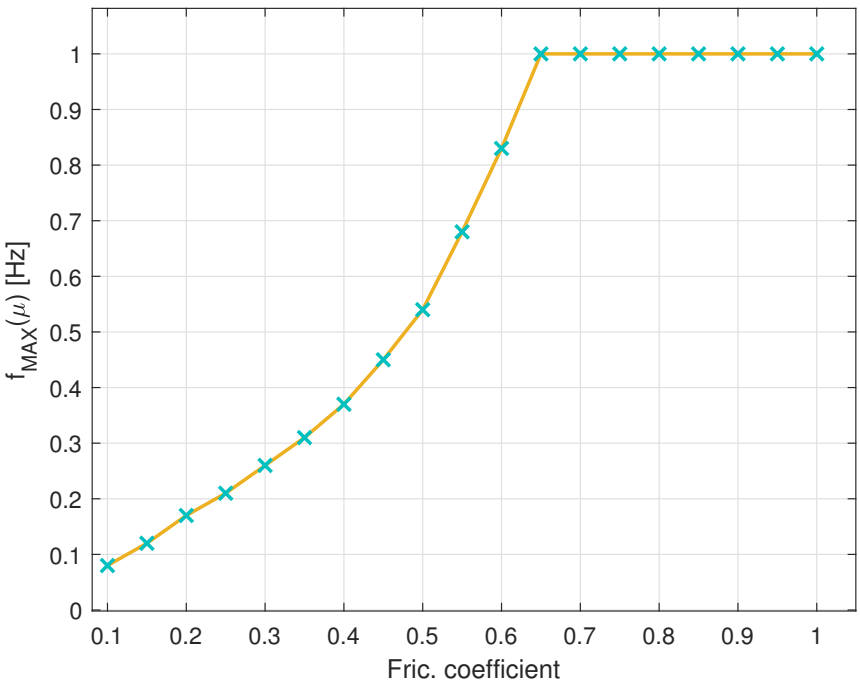

Figure 5.3: Map of the parameter $f_{MAX}(\mu)$.

5.2 Trajectory replanning

In this section, the sinusoidal trajectory generation is extended to be robust to unexpected grip changes, after a reference has been already given. The scope

is to guarantee that the controller can fast react to unfortunate situations where the friction coefficient suddenly decreases such as in case of dirt or snow on the road. This extension consists of a trajectory replanning, which has to be realized as soon as the friction change on the wheels (in particular, the frontal ones) is detected. To this scope, it is assumed that the vehicle is equipped with a grip estimator that can promptly sense the event.

The re-planned trajectory will be generated with an approach similar to the one of the previous section: it will be designed also in this case with sinusoidal waves and parts of constant curvature. Moreover, the same limitations on the maximum curvature are made, with the difference that the new friction coefficient μ_{new}, corresponding to the new road conditions, will be used in this case. To clarify how the replanning should work an example is shown in Figure 5.4: during the maneuver, the friction changes causing the given trajectory (gray dashed line) to be unfeasible, thus a feasible new sinusoidal trajectory is given to the controller.

Concerning how the new trajectory is built, some modifications has to be made to the expressions seen in the previous case. The vehicle has different initial conditions so the new expression of the curvature trajectory will become:

$$\rho(t) = \begin{cases} (\rho_1 - \rho_0)\sin\left(\frac{2\pi}{T_c}t\right) + \rho_0 & \text{if } \left[0, \frac{T_c}{4}\right] \\ \rho_1 & \text{if } \left[\frac{T_c}{4}, \frac{T_c}{4} + T_{12}\right] \\ \rho_1 \cos\left(\frac{2\pi}{T_c}\left(t - \frac{T_c}{4} - T_{12}\right)\right) & \text{if } \left[\frac{T_c}{4} + T_{12}, \frac{T_c}{2} + T_{12}\right] \\ \rho_2 \sin\left(\frac{2\pi}{T_c}\left(t - \frac{T_c}{2} - T_{12}\right)\right) & \text{if } \left[\frac{T_c}{2} + T_{12}, \frac{3T_c}{4} + T_{12}\right] \\ \rho_2 & \text{if } \left[\frac{3T_c}{4} + T_{12}, \frac{3T_c}{4} + T_{12} + T_{22}\right] \\ \rho_2 \cos\left(\frac{2\pi}{T_c}\left(t - \frac{3T_c}{4} - T_{12} - T_{22}\right)\right) & \text{if } \left[\frac{3T_c}{4} + T_{12} + T_{22}, T_c + T_{12} + T_{22}\right] \end{cases} \tag{5.7}$$

where the main difference with respect to 5.4 is the presence of ρ_0, which is the initial curvature at the replanning instant. This value will be computed based on the current state of the vehicle at the replanning instant t_{repl} and taking

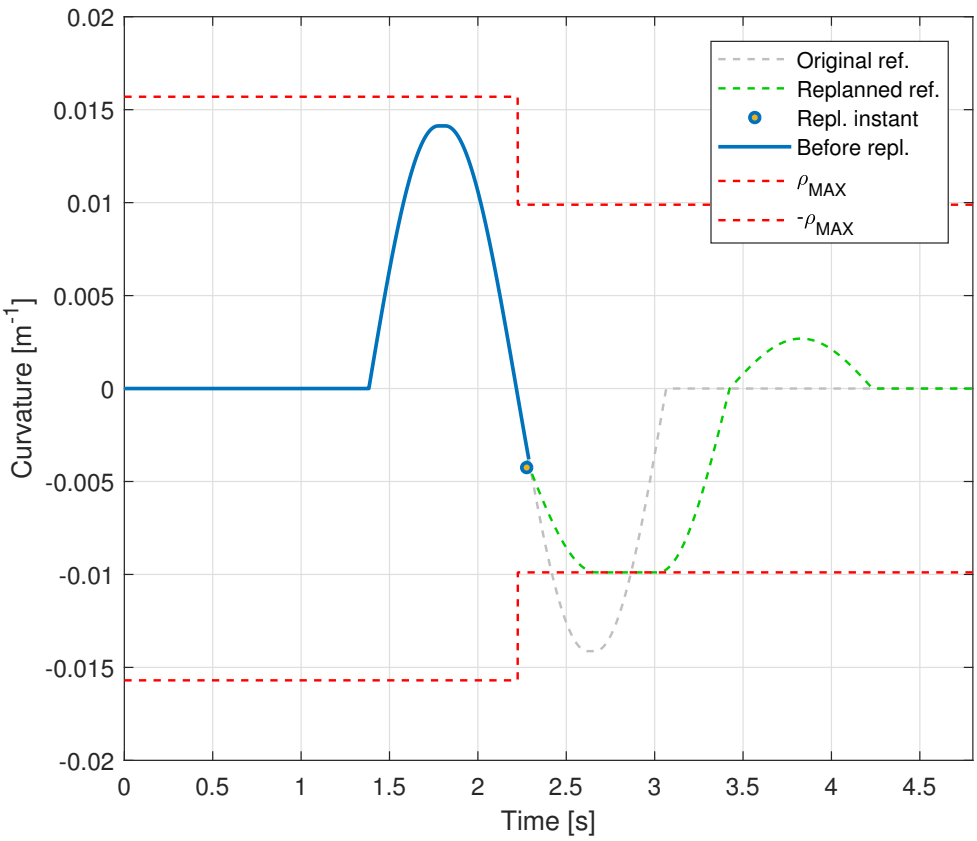

Figure 5.4: Example of replanning due to a change in the friction coefficient.

account of the curvature limitations. Similarly, also the expressions to compute the heading and the lateral displacement has to be slightly modified:

$$\begin{aligned} \psi(t) &= \int_{t_{repl}}^{t_{end}} V\rho(t)dt + \psi_0 \\ y(t) &= \int_{t_{repl}}^{t_{end}} V\psi(t)dt + y_0 \end{aligned} \tag{5.8}$$

where ψ_0 and y_0 are respectively the heading and the lateral displacement of the vehicle at the moment of replanning. By integration, it is possible to define the expressions of the final heading and lateral displacement and equal them to the requested final conditions:

$$\begin{aligned} \psi(t_{end}) &= \psi_0 + V\left(\frac{T_c}{\pi}(\rho_1+\rho_2) + \rho_1 T_{12} + \rho_0\frac{T_c}{\pi}\left(\frac{1}{2}-\frac{1}{\pi}\right) + \rho_2 T_{22}\right) = 0 \\ y(t_{end}) &= y_0 + V^2\left[\frac{1}{2}(T_{12}^2\rho_1 + T_{22}^2\rho_2) + \frac{7}{32}\rho_0 T_c^2 + \psi_0(T_{12}+T_{22}+T_c) + \right. \\ &+ T_{12}T_{22}\rho_1 + \frac{1}{4}T_{12}T_c\rho_0 + \frac{3}{4}T_{12}T_c\rho_1 + \frac{1}{4}T_{22}T_c\rho_0 + \frac{1}{4}T_{22}T_c\rho_2 + \\ &+ \frac{T_c^2}{2\pi}\left(-\rho_0 + \frac{3}{2}\rho_1 + \frac{1}{2\pi}\rho_0 + \frac{1}{2}\rho_2\right) + \\ &\left. + \frac{T_c}{2\pi}(-\rho_0 T_{12} - \rho_0 T_{22} + \rho_1 T_{12} + 2\rho_1 T_{22} + \rho_2 T_{22})\right] = y_{shift} \end{aligned} \tag{5.9}$$

As in the previous case, in 5.9 there are four unknowns ρ_1, ρ_2, T_{12} and T_{22} and only two equations to find them. In the case of sudden change of grip the controller has a very limited amount of time to react so use minimization algorithms is unrealistic. However, the subdivision in cases is more complex and a different approach is used to solve efficiently the system 5.9: eight basic solutions, that maximally exploits the limitations of the new road conditions, are used. Every solution is obtained by setting two of the unknowns with a fixed value and by solving the system using analytic expressions. The different settings are summarized in Table 5.1. The analytic expressions deriving from these conditions can be easily found offline and then used online without the need of recomputing them.

Table 5.1: Basic solutions used to re-plan the trajectory.

#	ρ_1	ρ_2	T_{12}	T_{22}
0	unknown	unknown	0	0
1	ρ_{max}	unknown	unknown	0
2	$-\rho_{max}$	unknown	unknown	0
3	unknown	ρ_{max}	0	unknown
4	unknown	$-\rho_{max}$	0	unknown
5	ρ_{max}	$-\rho_{max}$	unknown	unknown
6	$-\rho_{max}$	ρ_{max}	unknown	unknown
7	unknown	0	unknown	0

Notice that the *solution #0* corresponds to the trajectory made of pure sinusoidal waves. If this solution is feasible there is no need to investigate the others because it is for sure the one that requires less time to be performed. For this reason, this is always the first solution to be verified. While, if the *solution #0* is not feasible (i.e. the curvatures ρ_1 or ρ_2 exceed the maximum curvature $\rho_{max}(\mu_{new})$), then all the other seven solutions are computed and their feasibility is checked. Finally, the realizable solutions are compared by looking at the execution time $T_{tot} = T_c + T_{12} + T_{22}$ of each one and the fastest solution is taken. Notice that this algorithm is computationally efficient because all the solutions are found using analytic expressions. Therefore the delay can be considered mainly given by the time requested by the grip estimator to detect the change of the road conditions.

5.3 Replanning validation

Here the trajectory replanning strategy is tested in simulation using the Curvature Preview controller. The scope of this section is, in particular, to verify if

this strategy could improve the normal path tracking in case of unexpected grip changes and to understand which are the eventual limitations.

The validation is conducted by comparing the cases where the lane change is performed without modifying the trajectory and the simulations that use the replanning strategy. In this way, it is possible to verify if the replanning strategy works and if brings improvements to the use of the only path tracking controller. All the following simulations have in common the same starting condition: the vehicle is stable, it is going straight and it has to perform a lane change; the speed is kept constant at 90 km/h; the Curvature Preview controller is used as control strategy and it is fed with a trajectory that is feasible in nominal conditions (dry asphalt, $\mu = 1$). At a certain point in the lane change, a deterioration of the road conditions is assumed. The following set of cases is tested: the road conditions can change both at the beginning or in the middle of the maneuver; while the friction coefficient is decreased from $\mu = 1$ to both $\mu = 0.7$ and $\mu = 0.5$. In this section, the replanning is assumed to be immediate and thus no delay due to the grip change recognition is considered.

In Figure 5.5 it is shown the first test where the friction coefficient changes to 0.7 as soon as the lane change maneuver starts. The solution without replanning is not able to track the given reference and the vehicle is not kept stable as it is possible to notice by looking at the oscillations of the steering angle and at the increasing slip angle. Instead, the maneuver performed with the replanning can keep the vehicle stable and execute safely the lane change. Moreover, this happens with a maximum error of only 0.17 m. The non-feasibility of the original maneuver can be understood by looking at the expected kinetic acceleration of the original reference (gray dashed line) that is exceeding the physical limits of the lateral acceleration (red dashed line), differently from the one produced by the replanned trajectory (black dashed line).

The simulation reported in Figure 5.6 is considering the same change in the friction coefficient, but in a different position: the road conditions changes in

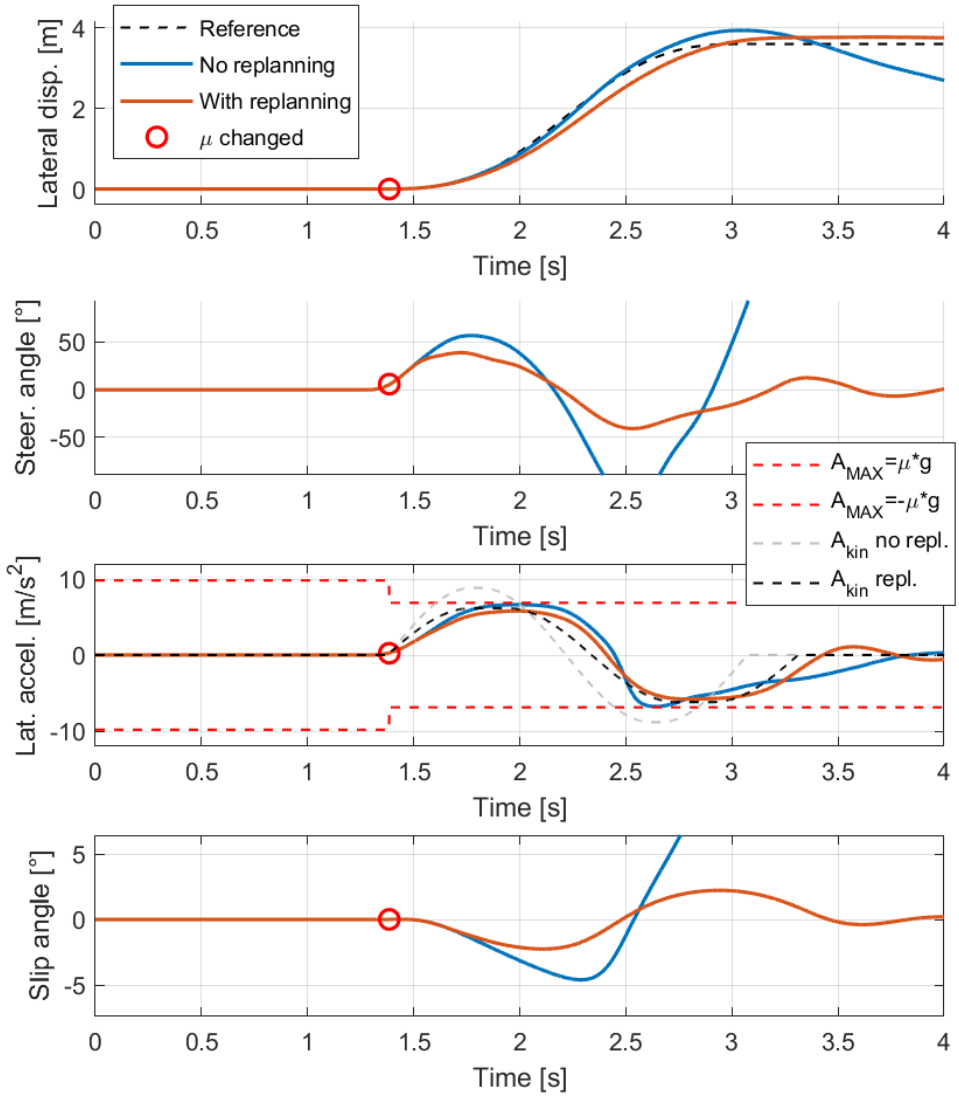

Figure 5.5: Comparison between lane change without replanning and with replanning. Change of friction coefficient at the beginning of the lane change from $\mu = 1$ to $\mu = 0.7$.

the middle of the lane change. Also this case demonstrates the importance of replanning the trajectory to successfully execute the lane change. However, in this case, the maximum lateral error is of 0.34 m, so it is doubled with respect to the previous case.

Now a higher friction change, from $\mu = 1$ to $\mu = 0.5$, is considered to see the performance of the replanning algorithm in more extreme conditions. The simulations of Figure 5.7 and Figure 5.8 respectively test this change in friction at the beginning and in the middle of the maneuver. In the first case, the replanning strategy allows the controller to track the given reference and keeping the error below 0.28 m. While, in the second one, although the expected kinetic acceleration of the replanned trajectory is inside the limits, the replanning algorithm fails and the vehicle becomes unstable.

As expected, it can be concluded that the replanning algorithm is giving improvements with respect to the solution that uses only the original trajectory, since it can keep the vehicle stable in some cases. However, if the difference between the new friction coefficient and the old one is too large the algorithm does not give the expected results. Moreover, it is found that the success of the maneuver is also dependent on the position in which is applied the change in the road conditions: in the middle of the curve is more difficult to have a successful replanning. An important remark should also be done on the fact that the unpredictability of the grip change makes the controller lose the advantage of exploiting the future information of the curvature reference. Indeed, before the replanning instant t_{repl} the controller is still fed with the advance of the old trajectory and only at t_{repl} it can have access to the information on the new path.

5.3.1 Sensitivity to replanning delay

Finally here is briefly discussed the importance of the delay τ in the replanning of the trajectory. This delay is assumed to be caused by the grip estimator and

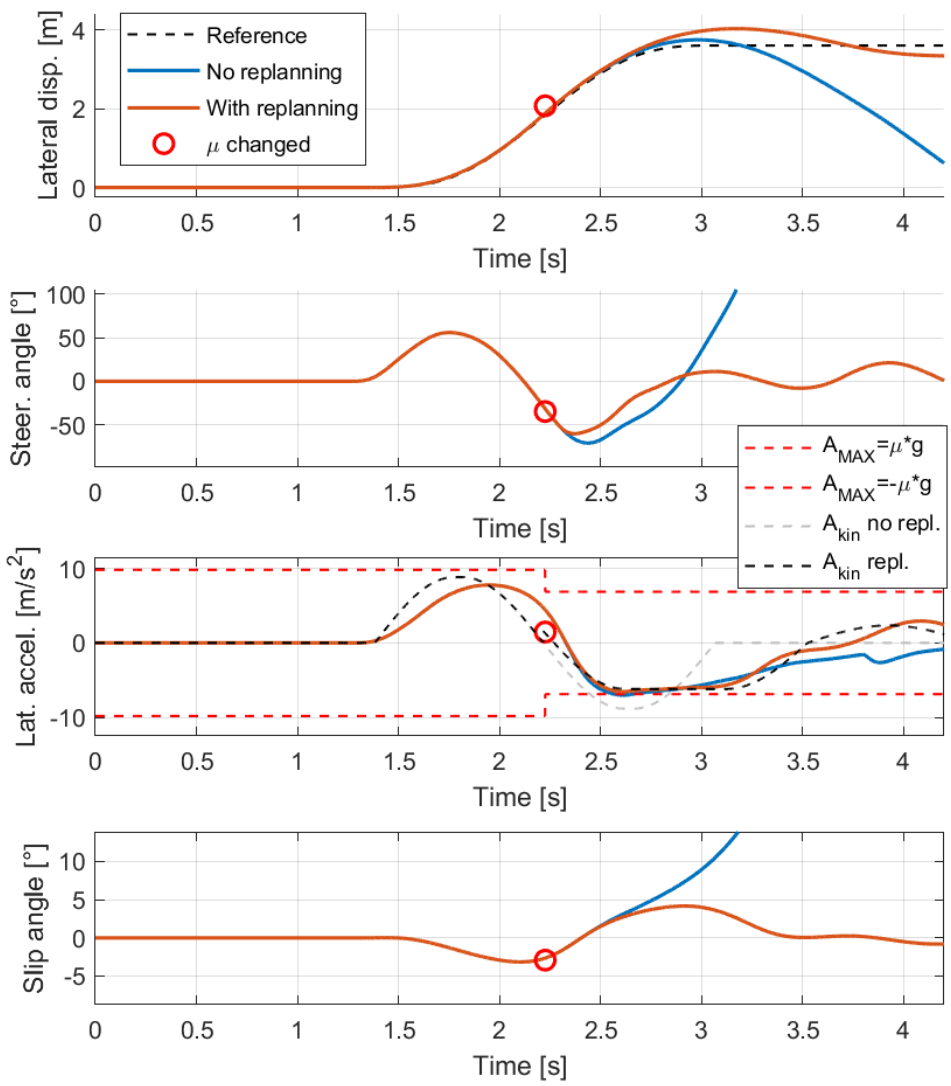

Figure 5.6: Comparison between lane change without replanning and with replanning. Change of friction coefficient in the middle of the lane change from $\mu = 1$ to $\mu = 0.7$.

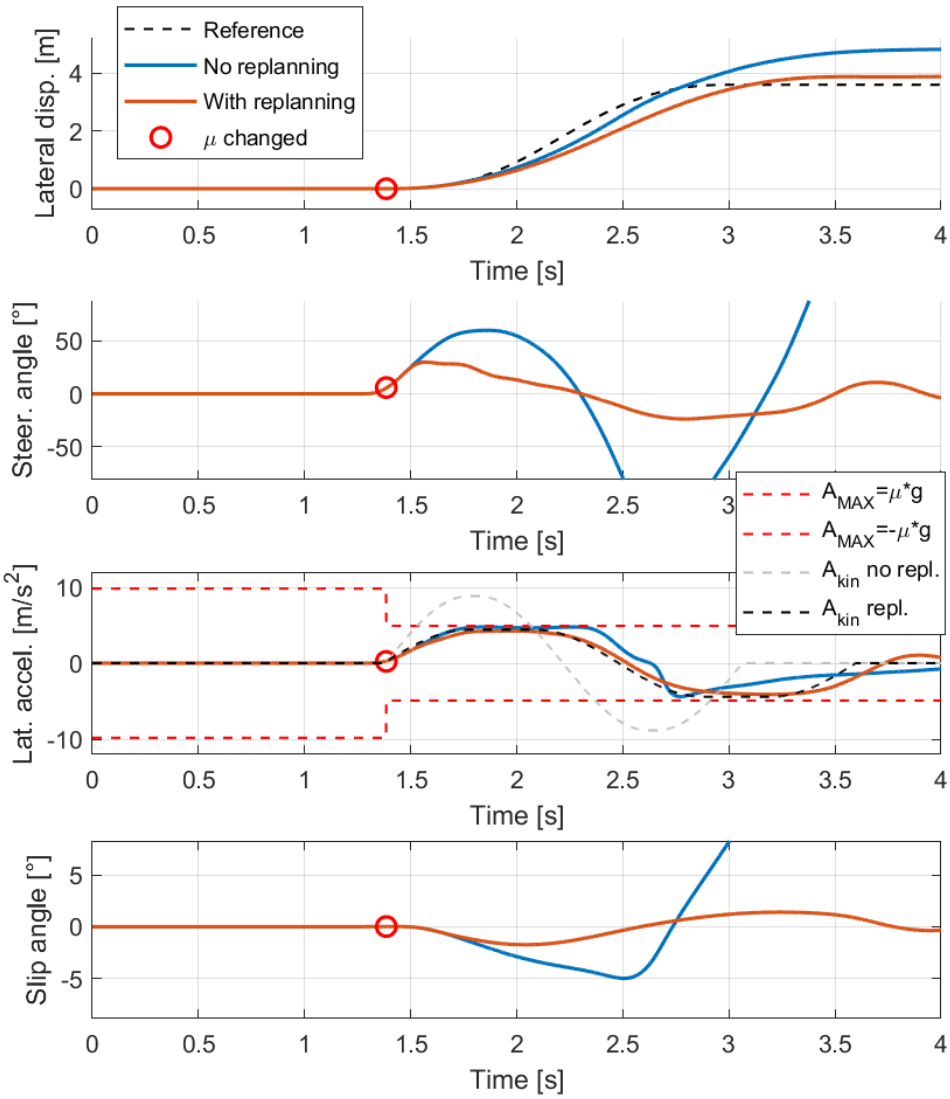

Figure 5.7: Comparison between lane change without replanning and with replanning. Change of friction coefficient at the beginning of the lane change from $\mu = 1$ to $\mu = 0.5$.

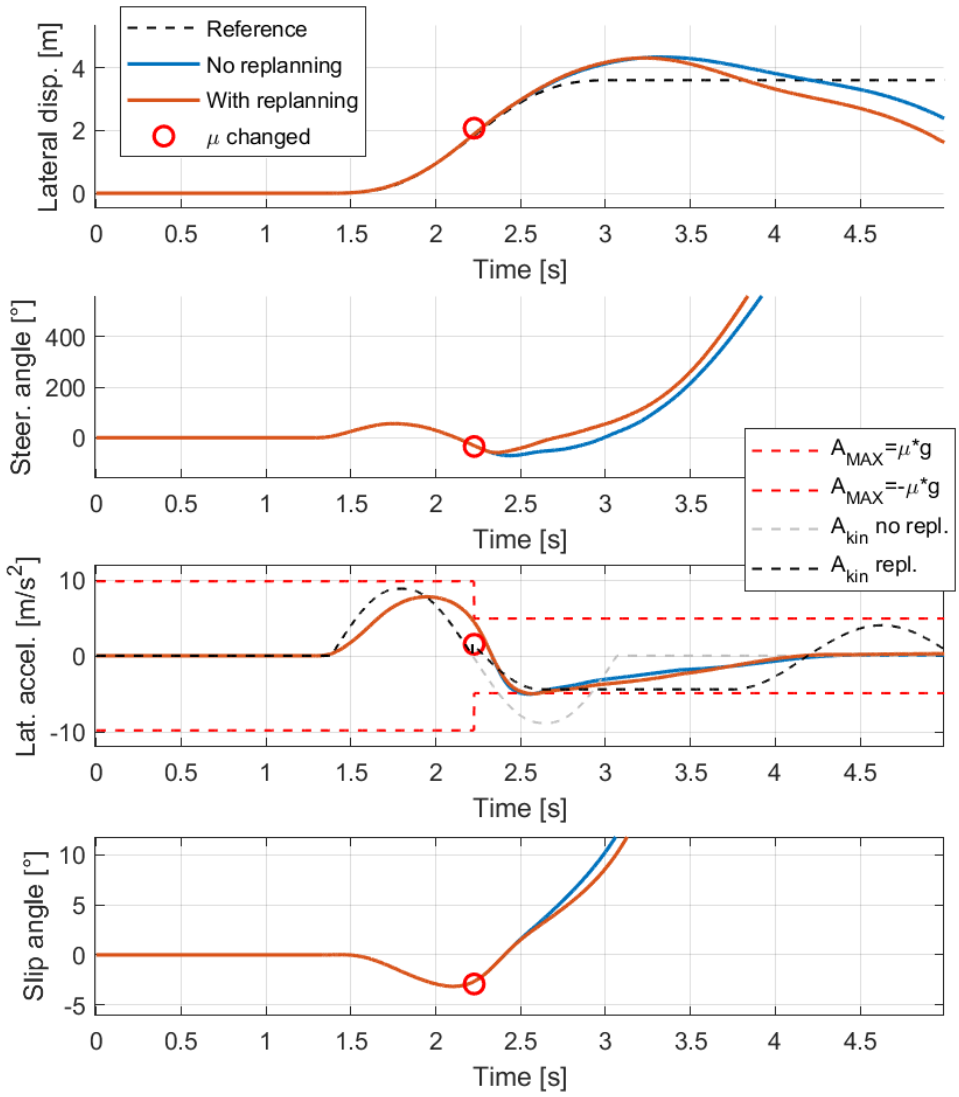

Figure 5.8: Comparison between lane change without replanning and with replanning. Change of friction coefficient in the middle of the lane change from $\mu = 1$ to $\mu = 0.5$.

it corresponds to the time to detect the event of the friction change. Once the detection is completed it is considered that the replanning computation by the trajectory planner can be almost instantaneous. Adding a delay in the simulation it was possible to find the maximum allowed τ_{max} to guarantee the success of the maneuver in the previously analyzed cases, in particular, these values can be found in Table 5.2.

Table 5.2: Maximum delays for different replanning simulations.

Position of μ variation	new μ	τ_{max} [s]
At the beginning	0.7	0.35
At the beginning	0.5	0.10
In the middle	0.7	0.05
In the middle	0.5	not possible

The reported delays vary a lot depending on the situations, however, it is possible to identify two main variables which affect their value: the new friction coefficient and the vehicle state during the change of road conditions. If the friction is lower the delay has to be more limited: it can be explained by considering that the limits of the lateral acceleration will be more stringent and will be easier to exceed them if the replanning is not fast enough. Also, if the vehicle is in the middle of the lane change the replanning has to be quicker. This can be probably caused by the different state of the vehicle during the maneuver.

Moreover to better understand how the maneuver performance is affected by the delay τ, in Figure 5.9 is reported a comparison between the instantaneous replanning, the replanning obtained using the maximum delay and a replanning with a delay slightly higher than the maximum one. It is possible to see that as the delay increases the final error increases too and the controller has problems to reject it.

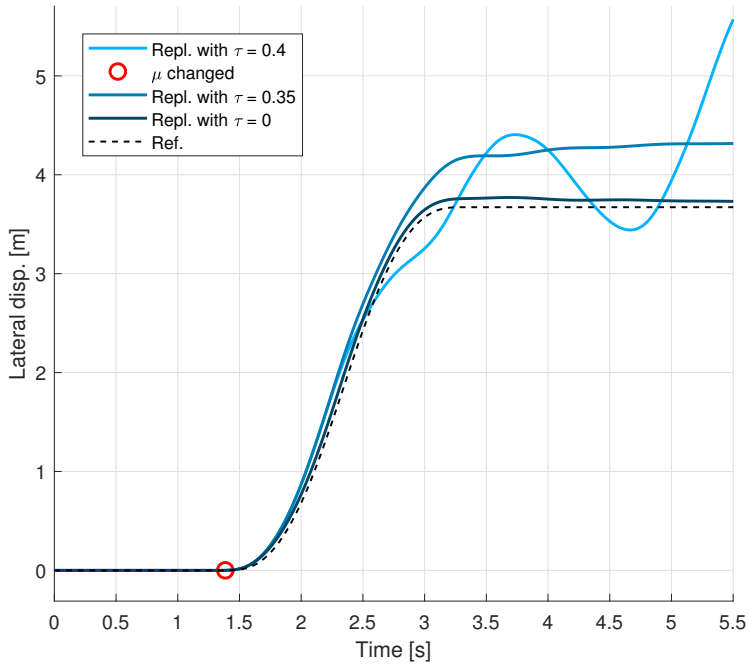

Figure 5.9: Sensitivity of the maneuver performance to different delay τ. Change of friction coefficient at the beginning of the lane change from $\mu = 1$ to $\mu = 0.7$.

5.4 Conclusions

It was presented the realistic problem of unexpected changes in the road conditions and it was suggested a possible solution based on an online replanning which not requires high computational effort. With this intention, the sinusoidal generation algorithm is extended to consider an initial generic condition and the new change in the curvature limitations. The main constraints which are considered are:

- the bandwidth of the controller;
- a maximum frequency parameter dependent on the friction coefficient;
- the maximum curvature ρ_{max};
- the final heading and the target lateral shift;

Finally, a validation of this algorithm is performed: assuming a high-quality grip estimator this algorithm can be used in case of moderate friction changes, such as from $\mu = 1$ to $\mu = 0.7$. If the alteration of the road does not happen in critical instants of the maneuver it is even possible that the replanning algorithm gives good results to more extreme friction changes, e.g. from $\mu = 1$ to $\mu = 0.5$. It can be concluded that the replanning algorithm is giving partially the expected results: it works but with some limitations, which mainly depends, as expected, on the delay and on the moment of the maneuver in which the replanning is executed. Remarkably, it was not found a case where the replanning strategy gives worse results with respect to the case where the replanning is not exploited.

Chapter 6

Conclusions

This dissertation dealt with the problem of the vehicle lateral control in an autonomous electric car focusing on two different issues: the path tracking and the trajectory generation.

Initially, an analysis of the vehicle was done and all the models of the actuators, of the single-track and of the lateral error dynamics were presented. From the study of the literature, two controllers were introduced and an improved structure was proposed. In particular, a first classic controller was realized based on the transfer function between the steering wheel angle and the lateral error. While the second more sophisticated one includes: a regulator to control the yaw rate, one to control the lateral error and an important curvature filter that allows the controller to exploit a preview of the trajectory. The simulations in CarMaker demonstrate that the use of the future information and of the double loop is of key importance to obtain better performances: the Curvature Preview Controller can indeed complete the reference maneuvers achieving a small lateral error also at the highest speeds. The Double Lane Change is correctly performed in nominal conditions up to 90 km/h, to which corresponds a lateral error of only 0.17 m; while the Obstacle Avoidance maneuver can be performed safely up to 50 km/h, to which corresponds a lateral error of 0.23 m.

By performing a sensitivity analysis to the friction coefficient it was found a dependence between the vehicle transfer function and the parameter μ. The controller was tested in simulation (in particular $\mu = 0.5$ and $\mu = 0.7$) and it was demonstrated that the considered controller is not robust to friction changes.

Then, a trajectory planning algorithm was presented, in which it was taken into account the bandwidth of the controller and a frequency value which is dependent on the friction coefficient μ. This strategy consists of giving as reference a curvature composed of pieces at constant curvature and by sinusoidal links.

It was proposed an extension of this algorithm for the replanning in situations of an unexpected change of the grip. The replanning is realized assuming the presence of a grip estimator and by considering the state of the vehicle in the moment of the change in the road conditions. This strategy was tested in simulation and it was found that the replanning is undeniably an improvement with respect to the case without it, however, there are some limitations to the success of the replanning maneuver depending on the position in which the friction changes, the entity of this change and the delay.

6.1 Future Work

An important first step is the validation of the results of this thesis in real experiments to verify if the models used to design the controllers are enough to describe the vehicle dynamics or if other more accurate models should be used. Moreover, the work in this thesis leaves a lot of space for future other developments and, in particular, it can be modified the Curvature Preview controller to be more robust to changes in the friction coefficient.

Bibliography

[1] John Sousanis. World vehicle population tops 1 billion units. *Wards Auto*, 15, 2011.

[2] World Health Organization. *Global status report on road safety 2018*. World Health Organization, 2018.

[3] Sebastian Thrun, Mike Montemerlo, Hendrik Dahlkamp, David Stavens, Andrei Aron, James Diebel, Philip Fong, John Gale, Morgan Halpenny, Gabriel Hoffmann, et al. Stanley: The robot that won the darpa grand challenge. *Journal of field Robotics*, 23(9):661–692, 2006.

[4] Alessandro De Luca, Giuseppe Oriolo, and Claude Samson. Feedback control of a nonholonomic car-like robot. In *Robot motion planning and control*, pages 171–253. Springer, 1998.

[5] Kirstin LR Talvala, Krisada Kritayakirana, and J Christian Gerdes. Pushing the limits: From lanekeeping to autonomous racing. *Annual Reviews in Control*, 35(1):137–148, 2011.

[6] Steven C Peters, Emilio Frazzoli, and Karl Iagnemma. Differential flatness of a front-steered vehicle with tire force control. In *2011 IEEE/RSJ International Conference on Intelligent Robots and Systems*, pages 298–304. IEEE, 2011.

[7] RS Sharp, Daniele Casanova, and P Symonds. A mathematical model for driver steering control, with design, tuning and performance results. *Vehicle system dynamics*, 33(5):289–326, 2000.

[8] M Thommyppillai, S Evangelou, and RS Sharp. Car driving at the limit by adaptive linear optimal preview control. *Vehicle system dynamics*, 47(12):1535–1550, 2009.

[9] Charles C MacAdam. Application of an optimal preview control for simulation of closed-loop automobile driving. *IEEE Transactions on systems, man, and cybernetics*, 11(6):393–399, 1981.

[10] Francesco Borrelli, Paolo Falcone, Tamas Keviczky, Jahan Asgari, and Davor Hrovat. Mpc-based approach to active steering for autonomous vehicle systems. *International Journal of Vehicle Autonomous Systems*, 3(2):265–291, 2005.

[11] Paolo Falcone, Francesco Borrelli, Jahan Asgari, Hongtei Eric Tseng, and Davor Hrovat. Predictive active steering control for autonomous vehicle systems. *IEEE Transactions on control systems technology*, 15(3):566–580, 2007.

[12] Alexander Katriniok and Dirk Abel. Ltv-mpc approach for lateral vehicle guidance by front steering at the limits of vehicle dynamics. In *2011 50th IEEE Conference on Decision and Control and European Control Conference*, pages 6828–6833. IEEE, 2011.

[13] Alexander Katriniok, Jan P Maschuw, Fréderic Christen, Lutz Eckstein, and Dirk Abel. Optimal vehicle dynamics control for combined longitudinal and lateral autonomous vehicle guidance. In *2013 European Control Conference (ECC)*, pages 974–979. IEEE, 2013.

[14] Ashwin Carvalho, Stéphanie Lefévre, Georg Schildbach, Jason Kong, and Francesco Borrelli. Automated driving: The role of forecasts and uncertainty—a control perspective. *European Journal of Control*, 24:14–32, 2015.

[15] Bo-Chiuan Chen, Cheng-Ting Tsai, Yu-Ming Lin, and Kangwon Lee. Design of an automated steering controller with steering actuator dynamics and adaptive preview time. In *Advanced Vehicle Control: Proceedings of the 13th International Symposium on Advanced Vehicle Control (AVEC'16), September 13-16, 2016, Munich, Germany*, page 163. CRC Press, 2016.

[16] F. Roselli. *Vehicle dynamics planning and control for safety and comfort in autonomous cars*. PhD thesis, Politecnico di Milano, 2017.

[17] Liang Ma, Jianru Xue, Kuniaki Kawabata, Jihua Zhu, Chao Ma, and Nanning Zheng. A fast rrt algorithm for motion planning of autonomous road vehicles. In *17th International IEEE Conference on Intelligent Transportation Systems (ITSC)*, pages 1033–1038. IEEE, 2014.

[18] Sébastien Glaser, Benoit Vanholme, Saïd Mammar, Dominique Gruyer, and Lydie Nouveliere. Maneuver-based trajectory planning for highly autonomous vehicles on real road with traffic and driver interaction. *IEEE Transactions on Intelligent Transportation Systems*, 11(3):589–606, 2010.

[19] Shohei Kitazawa and Tetsuya Kaneko. Control target algorithm for direction control of autonomous vehicles in consideration of mutual accordance in mixed traffic conditions. In *Advanced Vehicle Control: Proceedings of the 13th International Symposium on Advanced Vehicle Control (AVEC'16), September 13-16, 2016, Munich, Germany*, page 151. CRC Press, 2016.

[20] Simon Thompson and Satoshi Kagami. Continuous curvature trajectory generation with obstacle avoidance for car-like robots. In *International Conference on Computational Intelligence for Modelling, Control and Automation*

and International Conference on Intelligent Agents, Web Technologies and Internet Commerce (CIMCA-IAWTIC'06), volume 1, pages 863–870. IEEE, 2005.

[21] Xiaohui Li, Zhenping Sun, Qi Zhu, and Daxue Liu. A unified approach to local trajectory planning and control for autonomous driving along a reference path. In *2014 IEEE International Conference on Mechatronics and Automation*, pages 1716–1721. IEEE, 2014.

[22] Yanfeng Cong, Oliver Sawodny, Hong Chen, Jan Zimmermann, and Alexander Lutz. Motion planning for an autonomous vehicle driving on motorways by using flatness properties. In *2010 IEEE International Conference on Control Applications*, pages 908–913. IEEE, 2010.

[23] Zvi Shiller, Yu-Rwei Gwo, et al. Dynamic motion planning of autonomous vehicles. *IEEE Transactions on Robotics and Automation*, 7(2):241–249, 1991.

[24] Corrado Guarino Lo Bianco and Oscar Gerelli. Generation of paths with minimum curvature derivative with η^3-splines. *IEEE Transactions on automation science and engineering*, 7(2):249–256, 2009.

[25] Tim Mercy, Ruben Van Parys, and Goele Pipeleers. Spline-based motion planning for autonomous guided vehicles in a dynamic environment. *IEEE Transactions on Control Systems Technology*, 26(6):2182–2189, 2017.

[26] Dong Hun Shin, Sanjiv Singh, and W Whittaker. Path generation for a robot vehicle using composite clothoid segments. *IFAC Proceedings Volumes*, 25(6):443–448, 1992.

[27] Valerio Turri, Ashwin Carvalho, Hongtei Eric Tseng, Karl Henrik Johansson, and Francesco Borrelli. Linear model predictive control for lane keeping and obstacle avoidance on low curvature roads. In *16th international IEEE*

conference on intelligent transportation systems (ITSC 2013), pages 378–383. IEEE, 2013.

[28] Yiqi Gao, Andrew Gray, Ashwin Carvalho, H Eric Tseng, and Francesco Borrelli. Robust nonlinear predictive control for semiautonomous ground vehicles. In *2014 American Control Conference*, pages 4913–4918. IEEE, 2014.

[29] Joseph Funke, Matthew Brown, Stephen M Erlien, and J Christian Gerdes. Collision avoidance and stabilization for autonomous vehicles in emergency scenarios. *IEEE Transactions on Control Systems Technology*, 25(4):1204–1216, 2016.

[30] Dieter Schramm, Manfred Hiller, and Roberto Bardini. *Vehicle Dynamics: Modeling and Simulation*, chapter Single Track Models, pages 223–253. Springer Berlin Heidelberg, 2014.

[31] Hans B. Pacejka and Egbert Bakker. The magic formula tyre model. *Vehicle System Dynamics*, 1992.

[32] A. Gimondi and B. Tiralongo. Analisi e sviluppo di un sistema di controllo della dinamica laterale per un veicolo autonomo in condizioni di guida sportiva. Master's thesis, Politecnico di Milano, 2015.

[33] IPG Automotive GmbH. Carmaker. `https://ipg-automotive.com/products-services/simulation-software/carmaker/`, 2019.

[34] ISO 3888-1: 2018. Passenger cars – test track for a severe lane-change manoeuvre – part 1: Double lane-change, 2018.

[35] ISO 3888-2: 2011. Passenger cars – test track for a severe lane-change manoeuvre – part 2: Obstacle avoidance, 2011.

[36] Paolo Giuseppe Emilio Bolzern, Riccardo Scattolini, and Nicola Luigi Schiavoni. *Fondamenti di controlli automatici.* McGraw-Hill Education, 2015.

[37] Vincent A Laurense and J Christian Gerdes. Speed control for robust path-tracking for automated vehicles at the tire–road friction limit. In *14th International Symposium on Advanced Vehicle Control (AVEC). Beijing, China*, 2018.